United States Department of the Interior

Geological Survey

IN SITU DETERMINATION OF HEAT FLOW IN UNCONSOLIDATED SEDIMENTS

by

J. H. Sass, J. P. Kennelly, Jr., W. E. Wendt,

T. H. Moses, Jr., and J. P. Ziagos

Open-File Report 79-593

1979

Table of Contents

Figures

Figures (continued)

Tables

Plates

page

Abstract

Subsurface thermal measurements are the most effective, least ambiguous tools for identifying and delineating possible geothermal resources. Measurements of thermal gradient in the upper few tens of meters generally are sufficient to outline the major anomalies, but it is always desirable to combine these gradients with reliable estimates of thermal conductivity to provide data on the energy flux and to constrain models for the heat sources responsible for the observed, near-surface thermal anomalies. The major problems associated with heat-flow measurements in the geothermal exploration mode are concerned with the economics of casing and/or grouting holes, the repeated site visits necessary to obtain equilibrium temperature values, the possible legal liability associated with the disturbance of underground aquifers, the surface hazards presented by pipes protruding from the ground, and the security problems associated with leaving cased holes open for periods of weeks to months.

We have developed a technique which provides reliable "real-time" determinations of temperature, thermal conductivity, and hence, of heat flow during the drilling operation in unconsolidated sediments. A combined temperature, gradient, and thermal conductivity experiment can be carried out, by driving a thin probe through the bit about 1.5 meters into the formation in the time that would otherwise be required for a coring trip. Two or three such experiments over the depth range of,

say, 50 to 150 meters provide a high-quality heat-flow determination at costs comparable to those associated with a standard cased "gradient hole" to comparable depths. The hole can be backfilled and abandoned upon cessation of drilling, thereby eliminating the need for casing, grouting, or repeated site visits.

INTRODUCTION

Many of the alluvial and lacustrine valleys of the western United States have potential for the exploitation of geothermal energy. Of the various exploration techniques available, heat-flow drilling is the most direct and the least ambiguous, and exploration programs involving drilling patterns of holes to depths of between 10 and 500 meters have become common methods for discovering and delineating thermal anomalies. For these purposes, thermal gradients alone generally are sufficient. However, if the thermal conductivity can be characterized, the temperature gradients can be converted to heat-flow estimates, which, in turn, provide valuable information concerning the energy budget, and can be used to constrain hypotheses on the ultimate sources of the anomalous heat.

One of the main problems in obtaining useful data on the thermal conductivity of unconsolidated sediments results from the high cost and difficulty of recovering suitable core samples. In many prospects, repeated core runs produce little or no core and what little is recovered may not be representative of the formation. Even when extreme care is taken in handling samples, irreversible changes in their mechanical nature may occur before the conductivity determinations can be made. The conductivities of the solid component can be measured on drill cuttings, but reliable values of porosity are necessary to convert these data into meaningful estimates of formation conductivity.

Another problem in the highly competitive geothermal exploration industry is that of the security of cased temperature-gradient/heat-flow holes. These holes must be left for a minimum of a few days and preferably for several weeks to months, to allow the thermal disturbance introduced by the drilling process to subside. During this period, it has not been uncommon to have unauthorized entry and "midnight logs" of holes drilled for geothermal exploration. A hole that has been left open for a few days to weeks may become artesian, leading to surface damage and/or contamination of aquifers. Pipes left standing above the ground on playa surfaces may also present a hazard to fast moving vehicles.

In this report, we describe a downhole heat-flow probe which eliminates most of the problems outlined above. It gives satisfactory determinations of both temperature gradient and thermal conductivity and hence of heat flow, in unconsolidated sediments, essentially in real time. Because formation temperatures are measured below the bit during the drilling operation, the hole need not be cased and can be backfilled immediately upon cessation of drilling. Thermal conductivities are measured *in situ* so that mechanical disturbances to the formation are kept to a minimum.

The first comprehensive field trials of the system were held in the Black Rock Desert (Figure 1) near Gerlach, Nevada, during September 1978. For all trials, the test medium was a fine-grained unconsolidated Pleistocene or Holocene lake sediment, typically clay-rich, but occasionally

having sandy layers a few cm thick. The results from 29 probe runs in 12 holes (GRA through GRK and GRZ, Figure 1) are described herein, and compared with conventional determinations of gradient, conductivity, and heat flow.

The following symbols and units are used in the remainder of this report:

T, temperature °C

t, time seconds

K, thermal conductivity, 1 HCU = 1 mcal cm^{-1} s^{-1} $°C^{-1}$

= 0.394 Wm^{-1} K^{-1}

q, heat flow, 1 HFU = 10^{-6} cal cm^{-2} s^{-1} = 42.8 mWm^{-2}

Temperature gradient, °C km^{-1} = mKm^{-1}

Pressure, 1 kPa = 0.145 psi

Acknowledgments: Arthur Lachenbruch originally suggested the technique and gave valuable advice at many stages. Our success in the field was due, in no small measure, to the patience and skill of John Clingan and Western Geophysical crew GT-3. Vaughn Marshall, Mary Lou Zoback, and Eugene Smith rendered valuable assistance in the field.

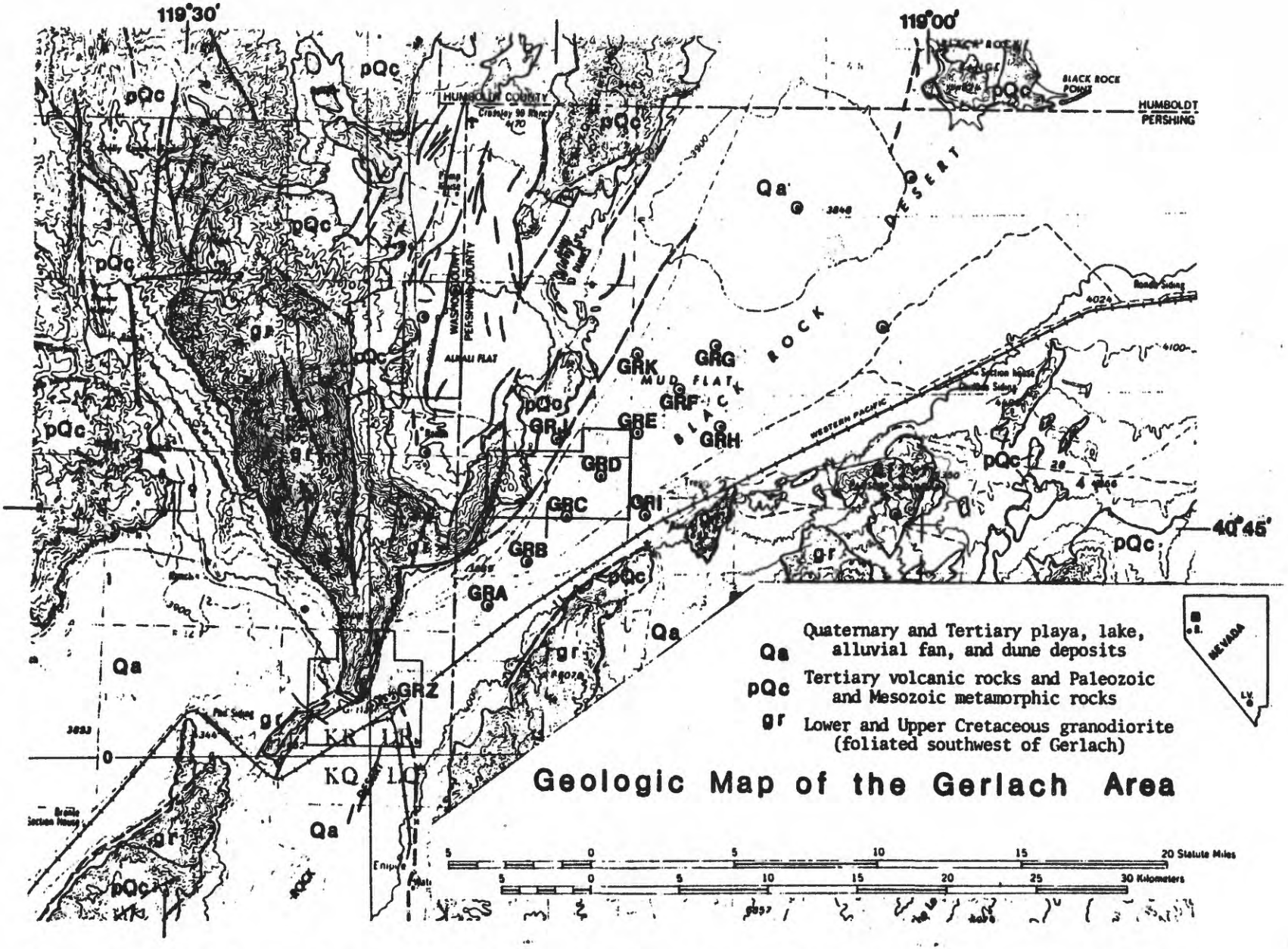

Figure 1. Geologic sketch map of Gerlach area showing the location of test wells. GRC and GRD are within the Gerlach NE KGRA. Inset: Map of Nevada showing location of study area relative to Reno (R) and Las Vegas (LV). Geology and faults generalized from Willden, 1964; Bonham, 1969; Olmsted and others, 1975; and Keller and Grose, 1978.

GENERAL DESCRIPTION OF THE SYSTEM

Figure 2 illustrates the essential features of a downhole probe test. At the depth selected for the test, the driller thickens his mud column and circulates for a few minutes to flush the cuttings out of the hole. The bit is then placed on bottom and a wireline pack-off assembly is connected to the drill string just above the rotary table. The probe is lowered into the drill stem until the piston on the driving mechanism enters the cylinder immediately above the bit (see Appendix C). The hydraulic pump on the logging truck then is activated, delivering water from a ∿150 liter capacity tank to the drill column. At the same time, the pack-off pump is used to tighten the packer assembly (Figure 2) to the point where only a small amount of fluid is leaking out of the top of the pack-off. When the cable moves downward a few cm, the water pressure is released to allow the return springs to move the "grabber" up the probe (Appendix C) and the column is pressurized again. This process is repeated until 1.65 m of penetration is achieved or until the pressures approach the mechanical strength of the probe (∿15000 kPa). During this period, the resistance of each thermistor is monitored at 20-second intervals and converted to temperature by the data-reduction program (see Appendix D). The temperature-time data are stored on magnetic tape, and a graph similar to those shown in Figures 3 and 4 is generated by the digital x-y plotter. The passive temperature record is run for 1500 seconds, typically allowing 1000 to 1200 seconds for the

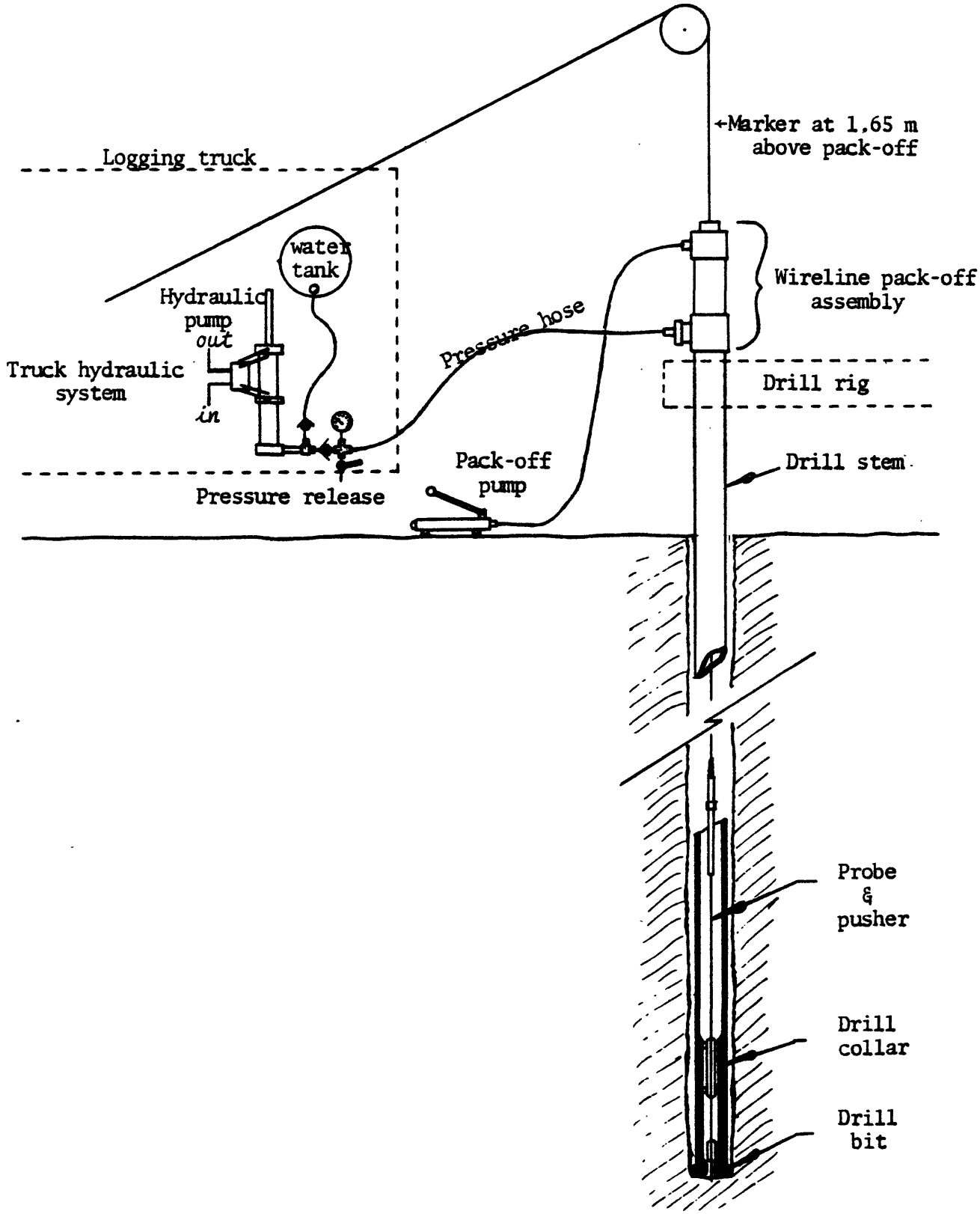

Figure 2. Schematic diagram of field setup for downhole probe experiment.

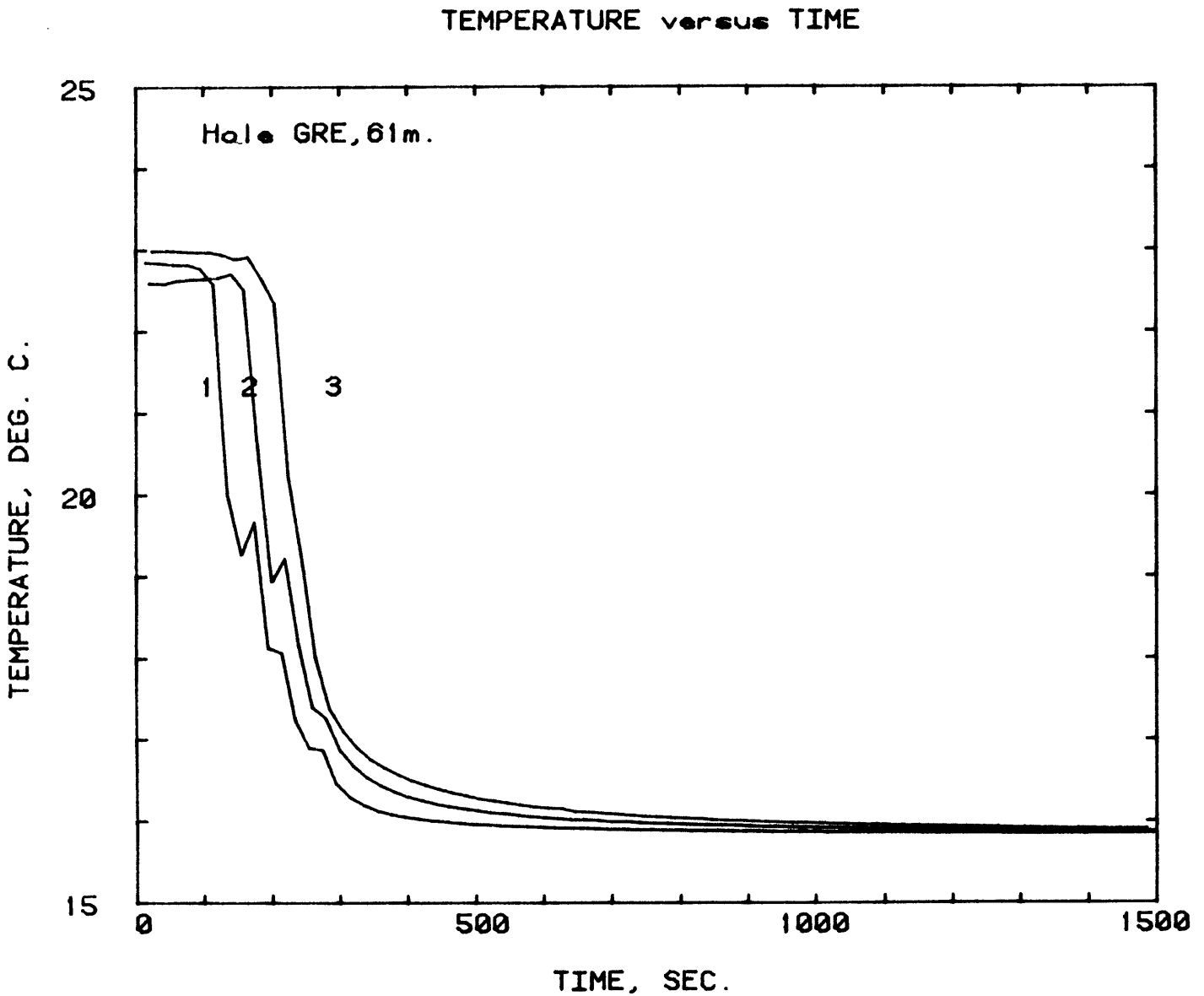

Figure 3. Temperature-time graph obtained during and after complete penetration of the downhole probe in Hole GRE. Numbers refer to probe thermistors, 1, lowermost. In this case, the drilling fluid is several degrees warmer than the formation.

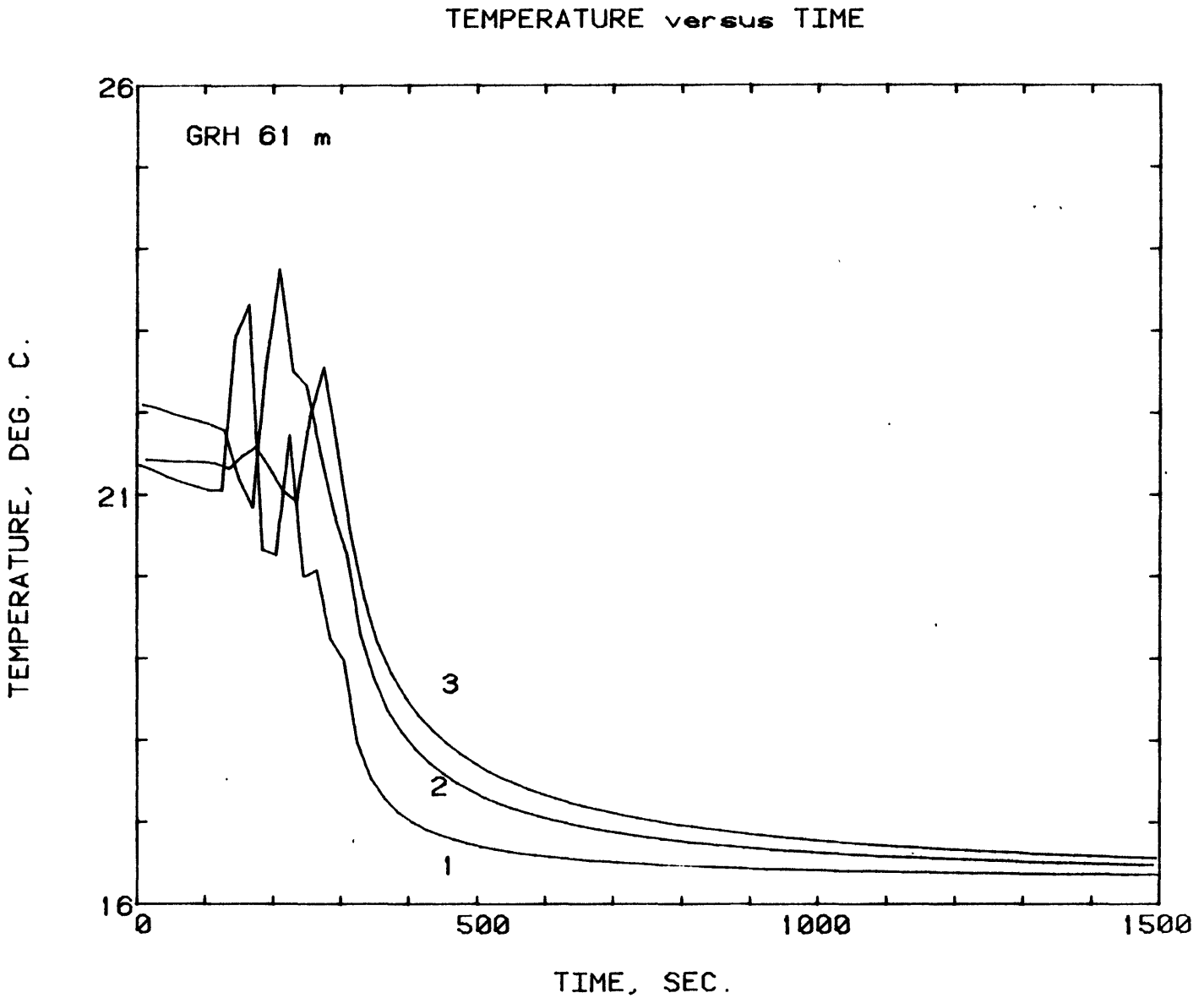

Figure 4. Another example of the temperature-time record for a complete penetration of the downhole probe.

decay of the thermal transient resulting from the friction between probe and formation. This time interval is not nearly sufficient to achieve thermal equilibrium, but when a smooth record is obtained (as in Figures 3 and 4), the data may be extrapolated to equilibrium values in a manner similar to that employed for the "Bullard" type of oceanic heat-flow probe (see Bullard, 1954; Langseth, 1965). One simple extrapolation scheme involves plotting temperature (T) as a function of 1/t (see Table 1, Lachenbruch and Brewer, 1959) where t is the elapsed time reckoned from approximately the midpoint of the penetration interval (about 225 seconds for Figure 3). This reduction is illustrated in Figures 5 and 6 for the corresponding curves in Figures 3 and 4. For time t large relative to the time taken to penetrate the formation; the curves should be linear, and indeed they are (Figures 5 and 6). Note also that even though the final measured temperatures are in reverse order (i.e., thermistor 3 hotter than 2 hotter than 1), the extrapolation to 1/t=0 provides (at least qualitatively) the expected increase in temperature with depth.

Upon completion of the passive temperature run (Figures 3 and 4) a constant current of about 100 mA is applied to the heater loop, the specific resistance of which is about $700\Omega\ m^{-1}$. The heat input to the formation is thus about 7 watts per meter of probe length. Representative temperature-log time curves are shown in Figures 7 and 8. The differences in temperature among the three thermistors are the result of differences in contact resistance between the heater and probe wall. For the probe

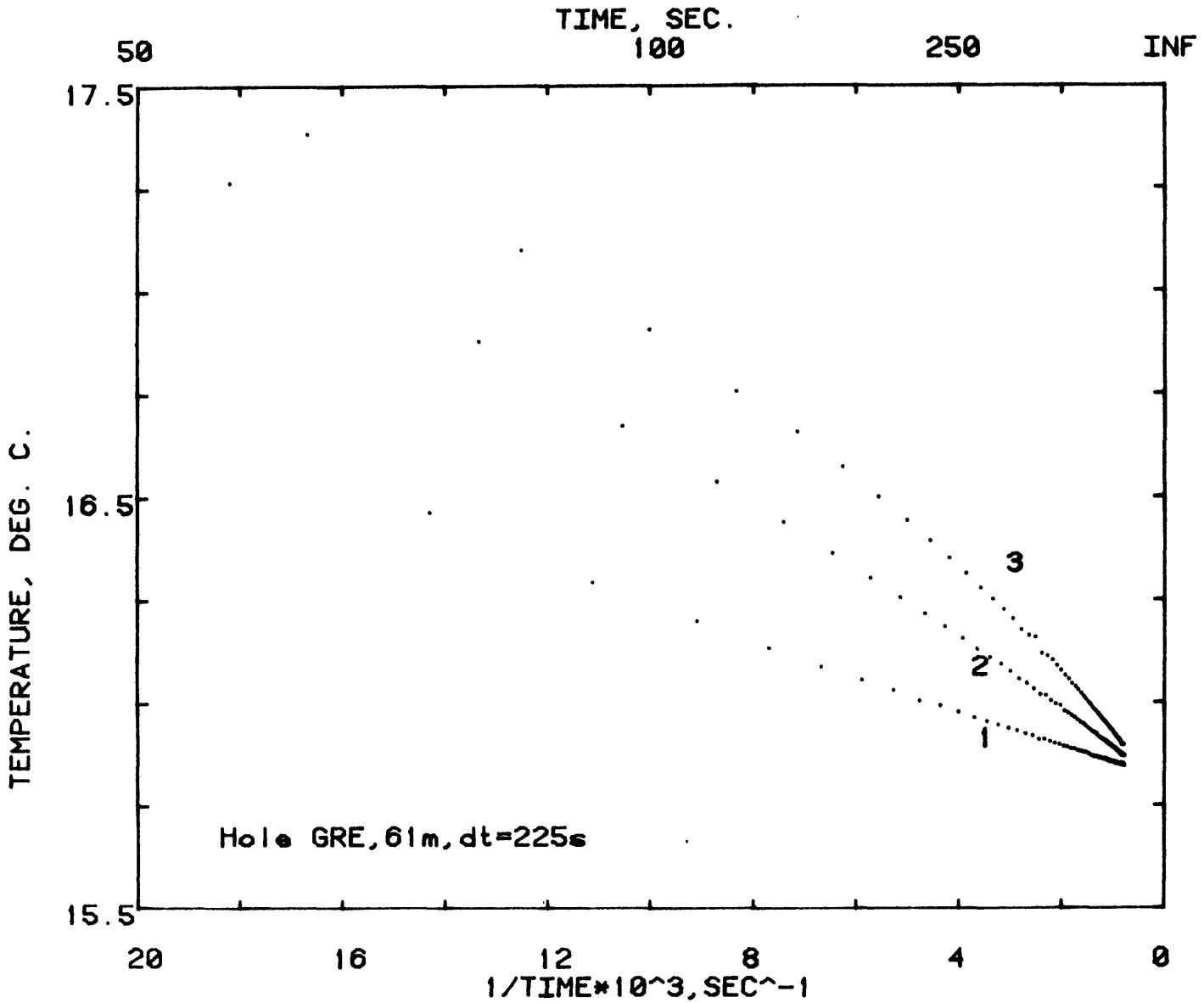

Figure 5. Temperature versus 1/time for the probe test shown in Figure 3.

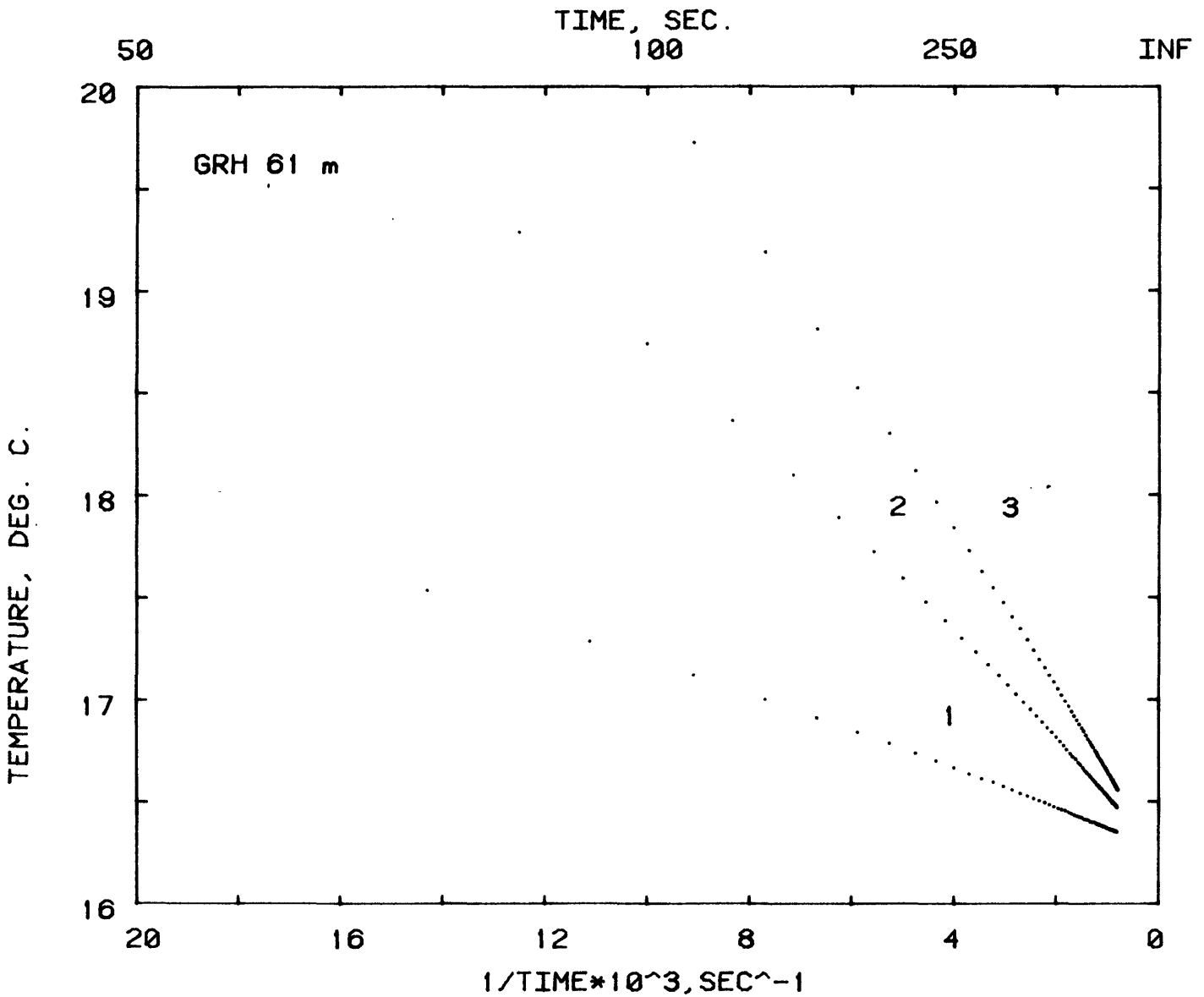

Figure 6. Temperature versus 1/time for the probe test shown in Figure 4.

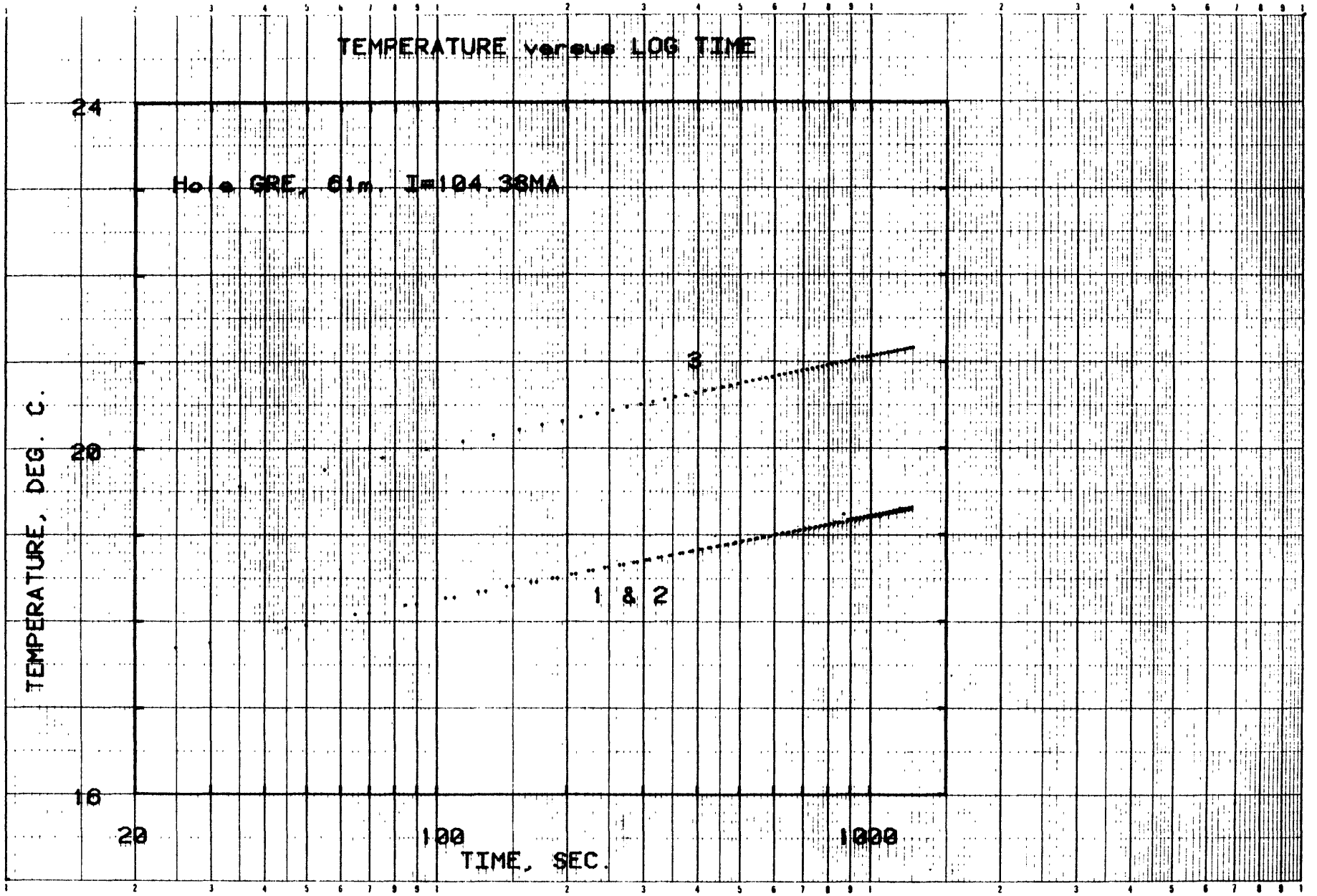

Figure 7. Conductivity run corresponding to the downhole test shown in figures 3 and 5

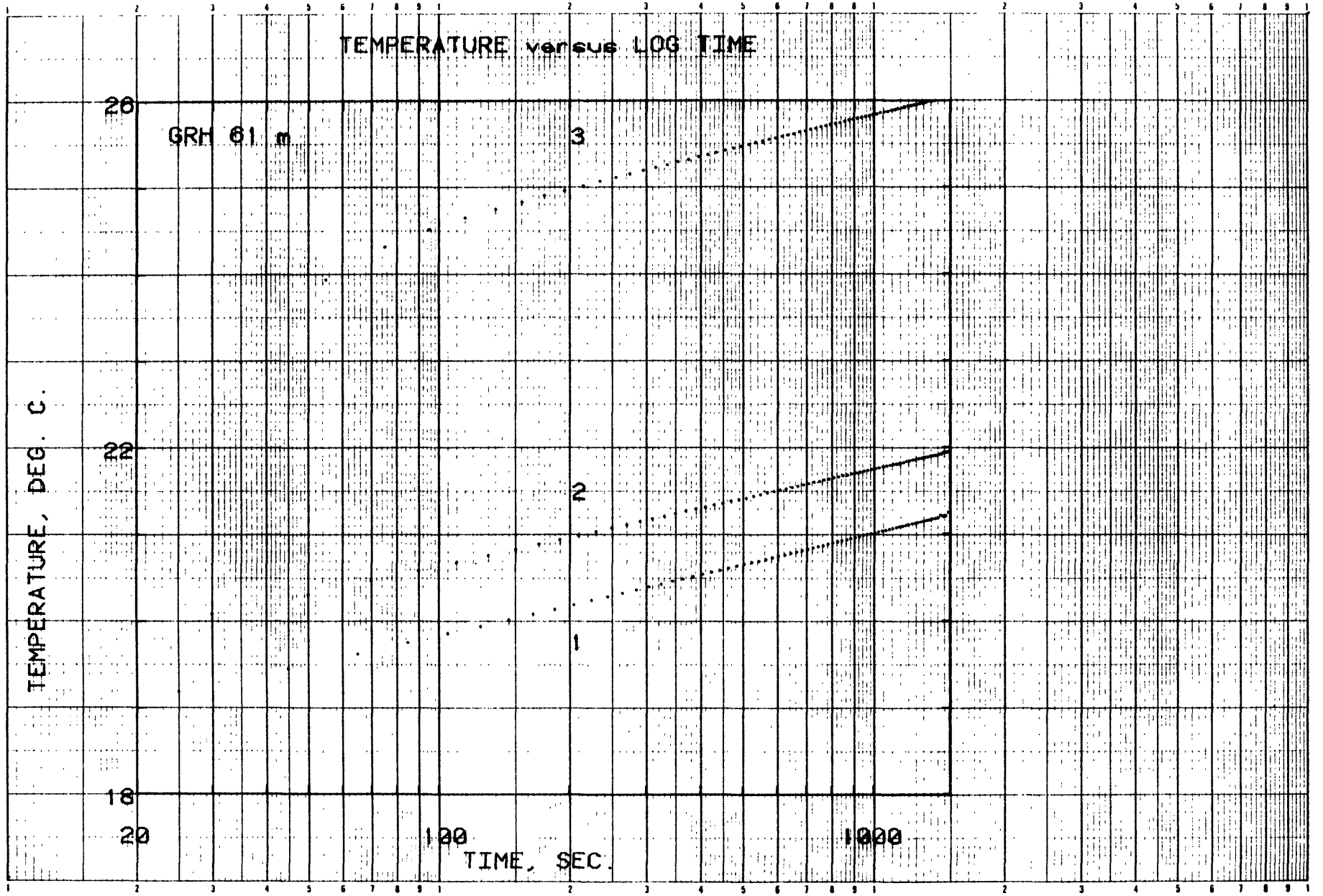

Figure 8. Conductivity run corresponding to the downhole test shown in Figures 4 and 6. Temperatures for thermistor 3 are 4°C higher than those shown on the ordinate axis.

used in GRH at 61 meters, there is evidently a fairly large air-filled void in the vicinity of thermistor 3 (Figure 8). The temperatures plotted in Figures 7 and 8 are not corrected for the rate of downward drift resulting from the decay of the thermal transients associated with frictional heating during penetration. The drift rate was calculated at the mid-point of the conductivity run (t ≈2000 sec) from the slope of the T versus 1/t lines (e.g., Figures 5 and 6) and a correction was applied to the observed temperature. This resulted in a small but significant increase in the slope of the T versus log t line (e.g., Figures 7 and 8) and consequently, a decrease on the order of 1% to 5% in the conductivity which is calculated from the expression

$$T(t) = \frac{Q}{4\pi K} \ell nt + 0(\frac{1}{t})$$

where Q is the rate of heating and K, the thermal conductivity (see Jaeger, 1958; Lachenbruch, 1957; Von Herzen and Maxwell, 1959). Upon completion of the conductivity test, the probe was removed by raising the entire drill string until the probe was completely out of the formation. Thereafter, the probe was raised to the surface by reeling in the cable and drilling was resumed.

In the first few holes, many probe tests were performed and cores were obtained to provide comparisons with *in situ* determinations of thermal conductivity. As the study progressed, however, we dispensed

with coring and settled on a scheme whereby probe tests were made at depths of 61 and 91 meters (200 and 300 feet). Total time required for insertion, 25 minute drift test, 15 to 20 minute conductivity test and retrieval of the probe was about an hour or roughly the time required for a coring trip at these depths. At one site (GRF, Figure A-6 and Table B-1), we established that the probe would penetrate fully at ∿120 meters (400 feet).

COMPARISON OF DOWNHOLE PROBE RESULTS WITH CONVENTIONAL MEASUREMENTS

Comparisons between probe and conventional determinations of temperatures, gradients, and thermal conductivities are shown in detail in Appendix B. The temperature comparisons also are summarized in the graphs of Appendix A. In this section we discuss briefly the various comparisons and some of their implications. The statistics for the relation $y=Ax$ where y is the probe value, and x the value derived from conventional measurements are shown in Table 1.

Thermal conductivity. Cores corresponding to the depths of the probe tests were obtained in hole GRZ (the first drilled); then in GRA, GRB, and GRC. At this stage, we were satisfied that the downhole conductivities were, in fact, comparable to those obtained conventionally, and coring was discontinued. The scatter is fairly small (Figure 9). The coefficient of correlation is 0.96 and downhole probe conductivities are systematically higher than those measured on core by about 5% (Table 1). We attribute this difference to slight structural changes in the core caused by the removal of the core from its environment and thus we prefer the downhole values (sufficient conductivities were measured along the axis of the core to confirm that there was no measurable anisotropy). The most striking example of physical changes occurred in the core from 30.5 to 32 meters in hole GRA (see Table B-1, Appendix B). When a hole was drilled into the wall of the core liner to allow access for the needle probe, there was a "pop" and a muddy slurry was extruded from the core. We see in this instance (Table B-1) that needle-probe conductivities are systematically lower than *in situ* values by about 10%.

TABLE 1. Coefficients of the least-squares regression line $y = Ax$ for the comparison between thermal parameters derived from downhole probe measurements (y) and those (x) determined by conventional methods*

Parameter	Correlation coefficient	A	RMS residual†
Conductivity	0.96	1.05	0.12 HCU
Temperature	1.00	1.00	0.04 °C
One-meter gradients	0.99	0.94	5.6 °C/km
Heat flow (1-m)	0.99	0.96	0.13 HFU
Heat flow (neighboring probe runs)	1.00	1.02	0.05 HFU

*"Equilibrium" temperature logs for temperatures and gradients; needle-probe determinations on core for thermal conductivity.

† $\left(\sum_{i=1}^{N} (y_i - Ax_i)^2/(N-2) \right)^{1/2}$

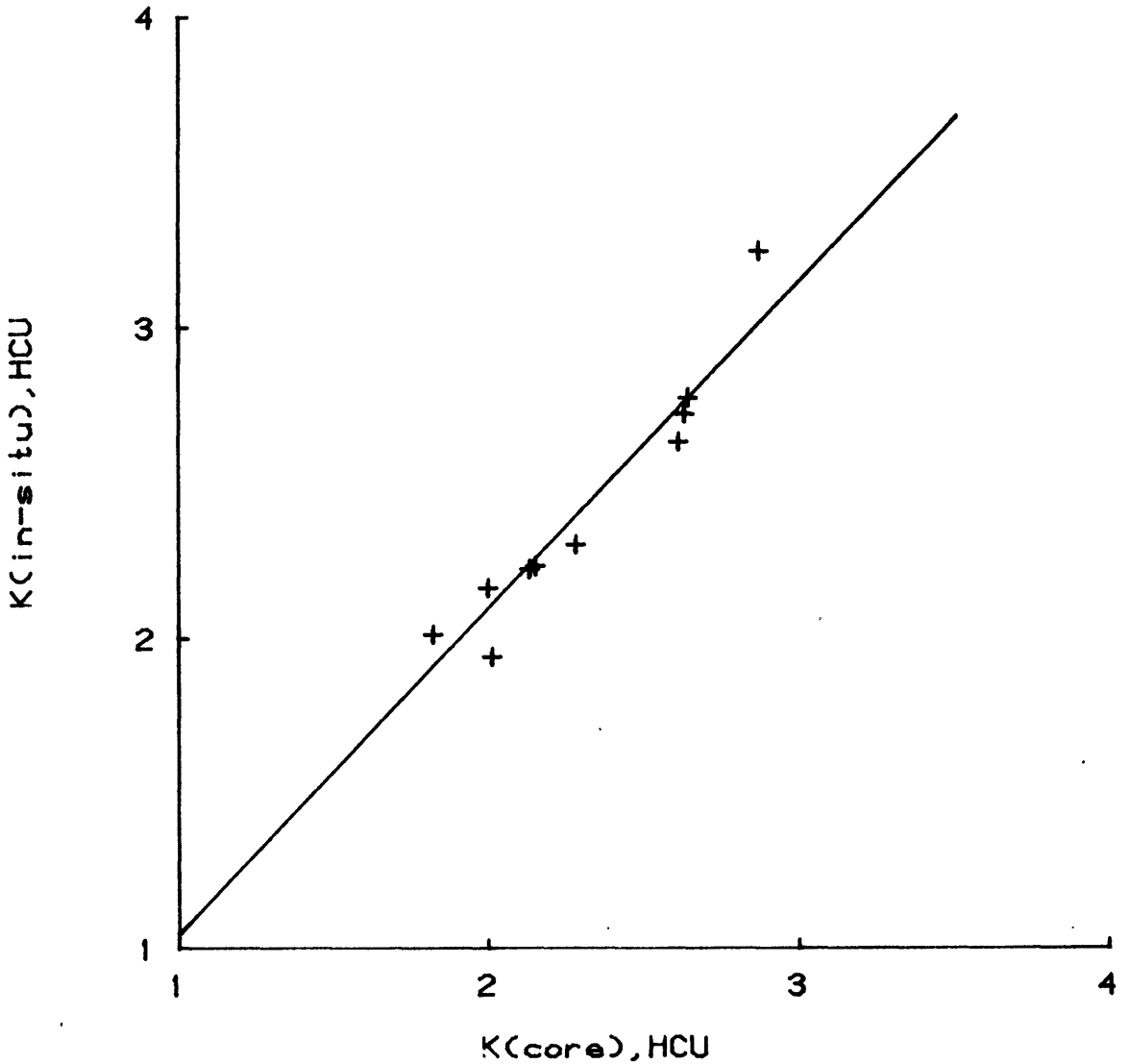

Figure 9. Comparison between average downhole probe conductivities over one meter and the corresponding averages for from 3 to 6 needle-probe determinations on core. (See Appendix B for details.)

Formation temperatures. Temperatures obtained from all probe runs by least-squares extrapolation of the later parts of the T versus 1/t lines (generally for the last 200 to 300 seconds) are plotted against temperatures at the same depth from the most recent temperature log in Figure 10. The correlation is excellent (Table 1) and the value for A of 1.00 tends to confirm our suggestion (Appendix B) that the temperature differences are random and are caused primarily by the uncertainty in depth-measurement.

Gradients over one meter. The largest source of uncertainty in obtaining gradients over a one-meter interval results from the $\sim$0.01°C resolution in relative temperatures between thermistors. Even though individual thermistors were calibrated to within a few millidegrees and the drift rate of each thermistor calibration is slow, small and unpredictable changes in calibration do occur. Calibrations were checked in the field by comparing each thermistor to a single thermistor mounted in a lagged aluminum cylinder. Departures (usually $\pm$ a few millidegrees) from calibration were noted and included in the temperature reduction part of the program so that all thermistor temperatures were relative to a common datum. Even with these procedures, our maximum possible error in the gradient over 1 meter is $\pm$20°C/km, clearly not accurate enough for "single point" determinations of regional heat flow, but certainly sufficiently sensitive to delineate the type of anomaly associated with possible sources of geothermal energy.

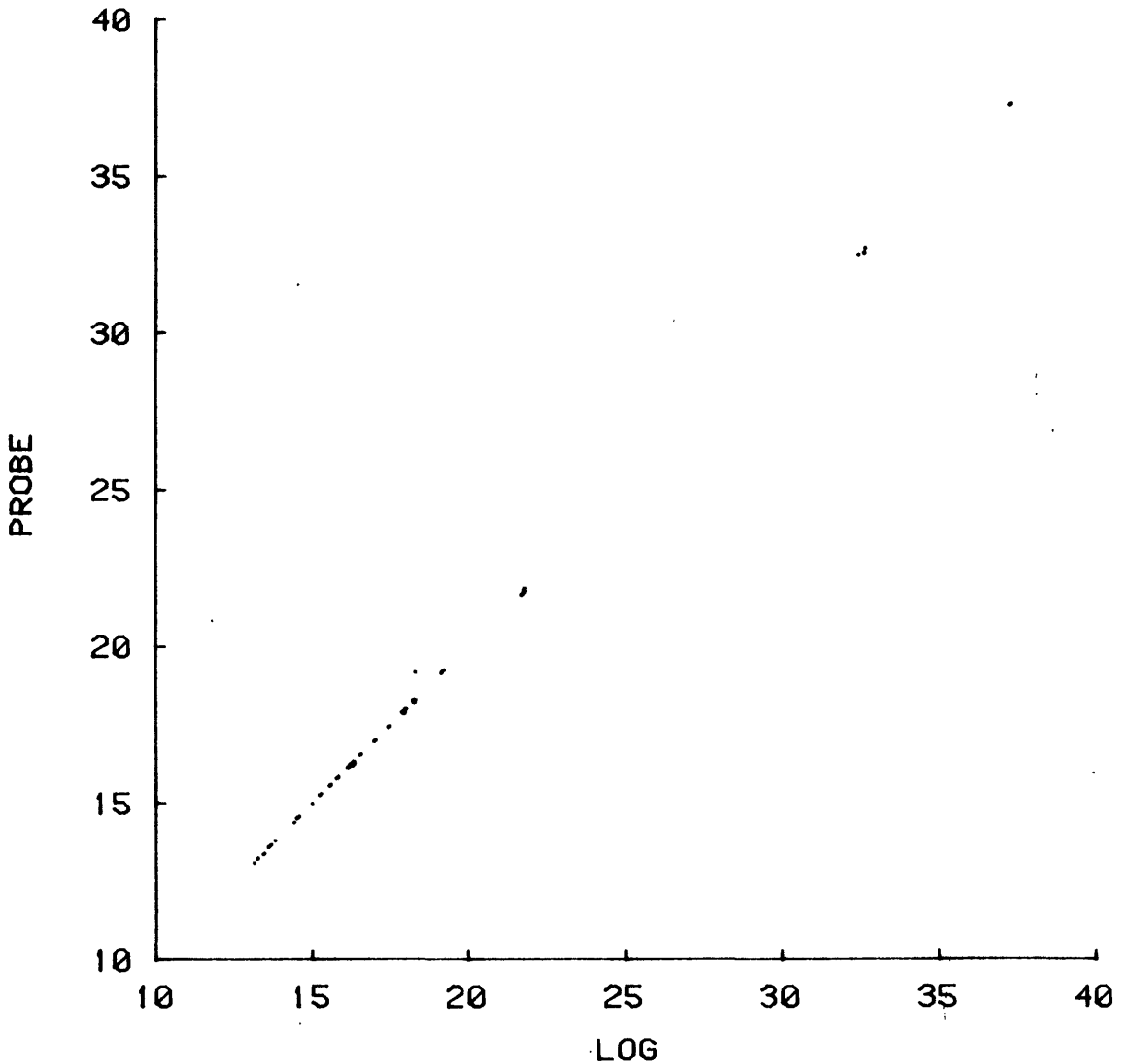

Figure 10. Formation temperatures deduced from downhole probe tests versus temperature at the same depth from the most recent temperature log. (See Appendices A and B for details.)

Although there is a fairly large scatter (Figure 11), one-meter gradients from the probe experiments correlate very well with those determined from least-squares fits to the six points from the most recent temperature log spanning the 1.5 meter interval penetrated by the probe (Table 1). Only results from complete penetrations were used in this comparison. Where only two thermistors entered the formation (Appendix B) the scatter was much greater. This should be expected, as we are attempting to measure the gradients over only 0.5 m and often the temperature of the uppermost thermistor (#2) is affected by the invasion of drilling fluid.

Heat flow. Since, in most instances, the downhole conductivities were used for both the probe and "conventional" heat-flow estimates over one meter, the same comments as those made with respect to the one-meter gradient determinations apply to the one-meter heat-flow determinations. Another approach to heat-flow determinations involves computing gradients and mean thermal conductivities over one or more intervals between probe runs. When intervals of a few tens of meters are used, the uncertainties due to reference levels and the errors of ± 0.01°C in relative temperatures become negligible. Only one thermistor need penetrate the formation for each run, something which was accomplished in every trial. With one exception (GRG, Figure 12) the heat-flow estimates over the larger intervals agree very well with those calculated from the most recent temperature log. The one exception, GRG, Figure A-7 and Table B-7, suggests that the downhole probe may be the superior technique quite apart from its other advantages.

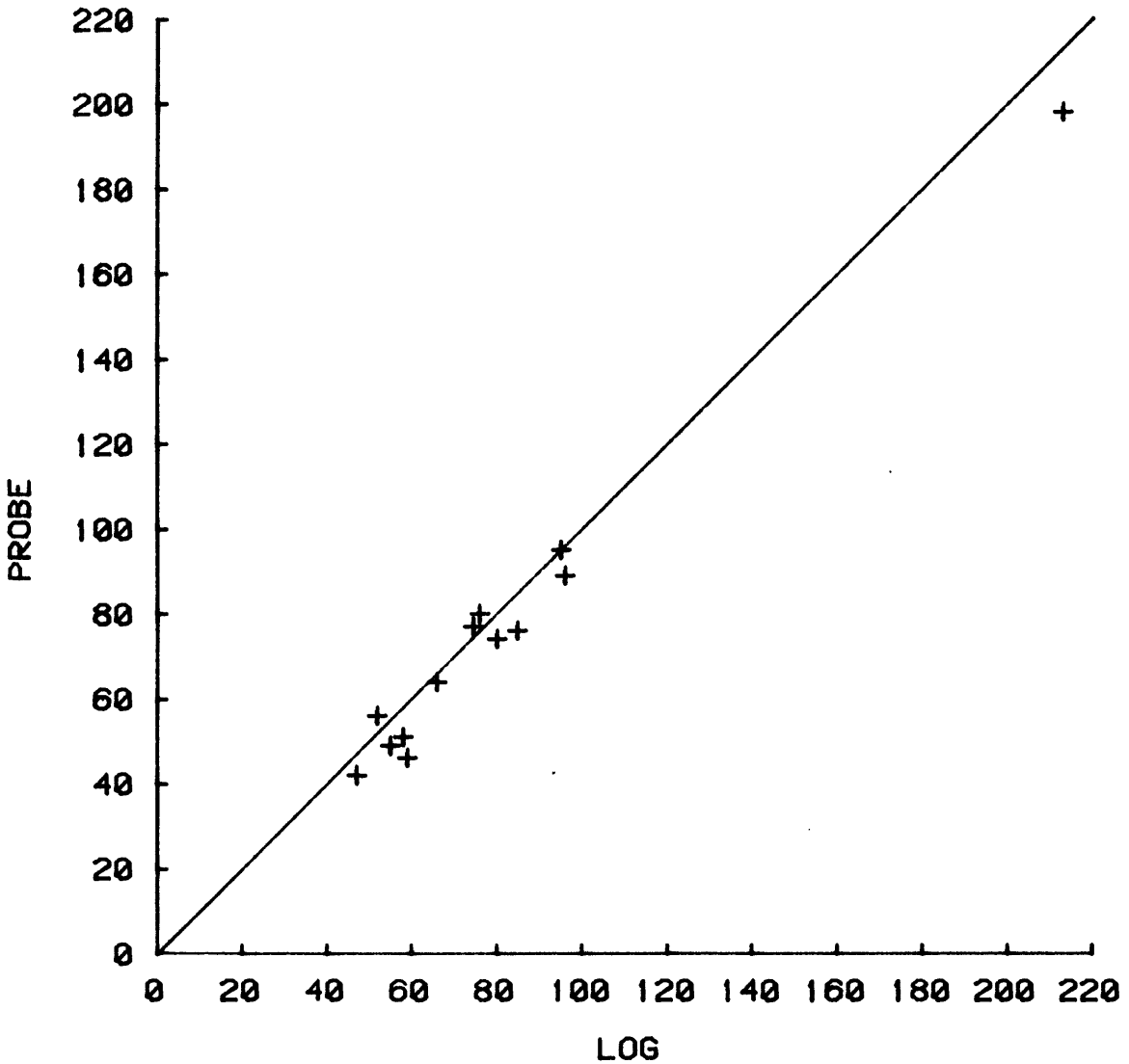

Figure 11. Gradients (°C/km) over 1 meter from probe experiments versus those determined from the most recent temperature log.

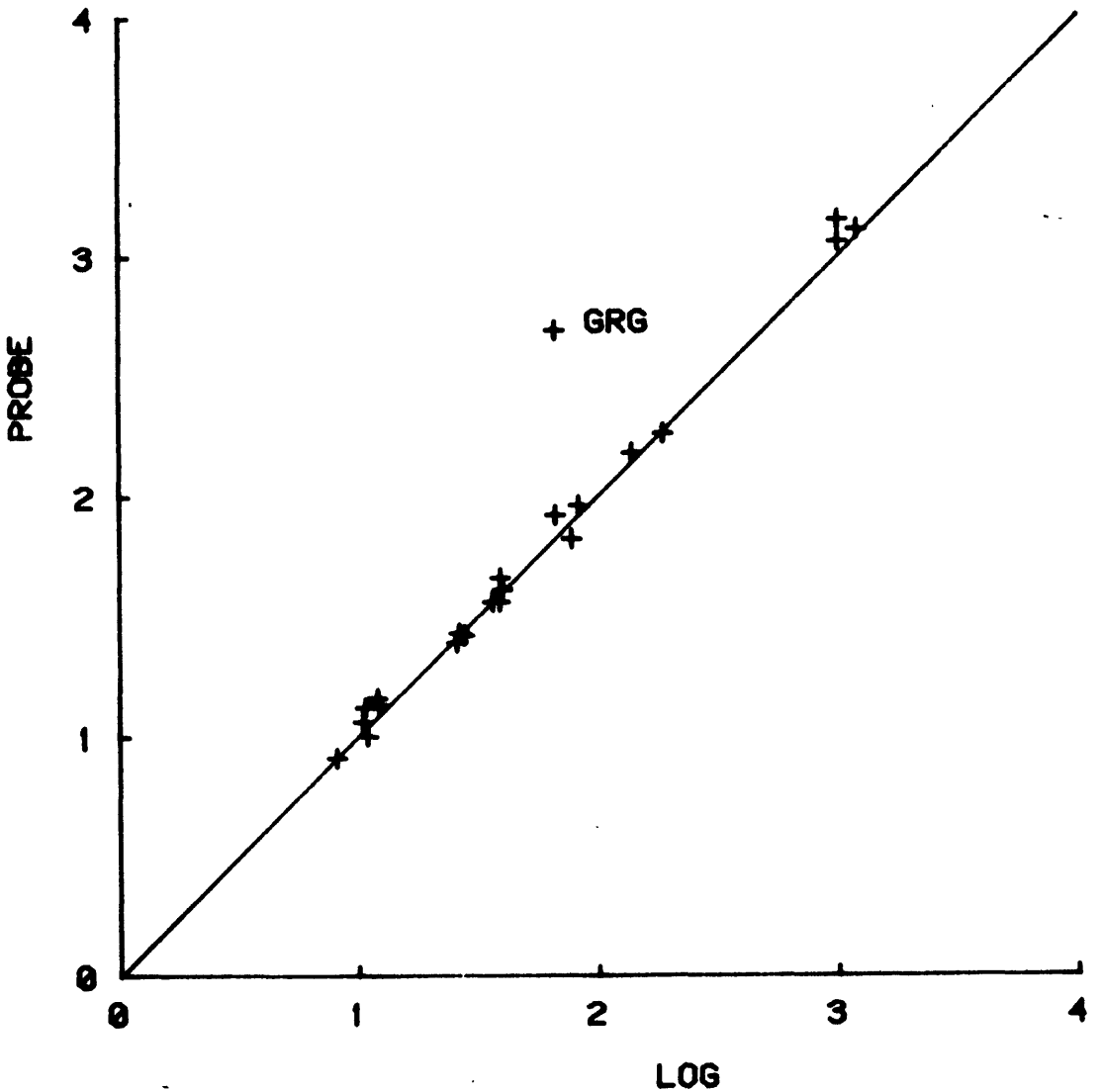

Figure 12. Heat flow (HFU) over intervals of between 6 and 60 meters determined between neighboring downhole probe runs versus heat flows determined from conventional temperature logs (see Appendix B for details).

For the probe test at 61 m in GRG, only two thermistors penetrated well into the formation (thermistor 3 was perhaps 2 cm, at most, 5 cm below the bit). When drilling resumed, the driller reported a hard sandy "stringer" a few cm thick just below 61 m. Maximum pressures and a long time (∿1000 sec) were required to get the probe into the formation. From the penetration record (Figure 13) thermistor 1 has repeated episodes of frictional heating whereas the temperature of thermistor 2 drops immediately as it enters the formation with a cooling curve quite different from either 1 or 3. Thermistor 3 is barely in and its decay curve is probably affected by interaction with the drilling fluid. It is curious and probably not coincidental that the extrapolated equilibrium temperature for thermistor 1 lies on the extension of the very smooth profile in the upper 60 meters (Figure A-7) whereas that for #2 lies precisely on the most recent temperature log which has some rather suspicious "bumps." Since there is no change in lithology between the upper and lower portions of the hole, it seems plausible that the drill opened a channel between two intervals with a slight head difference, and that water has been moving downward in the annulus since that time; this despite the fact that the section of the hole with the "funny profile" was apparently grouted off. This explanation might be applicable to other areas in which, within an apparently uniform lithology, an abrupt change in temperature gradient is observed.

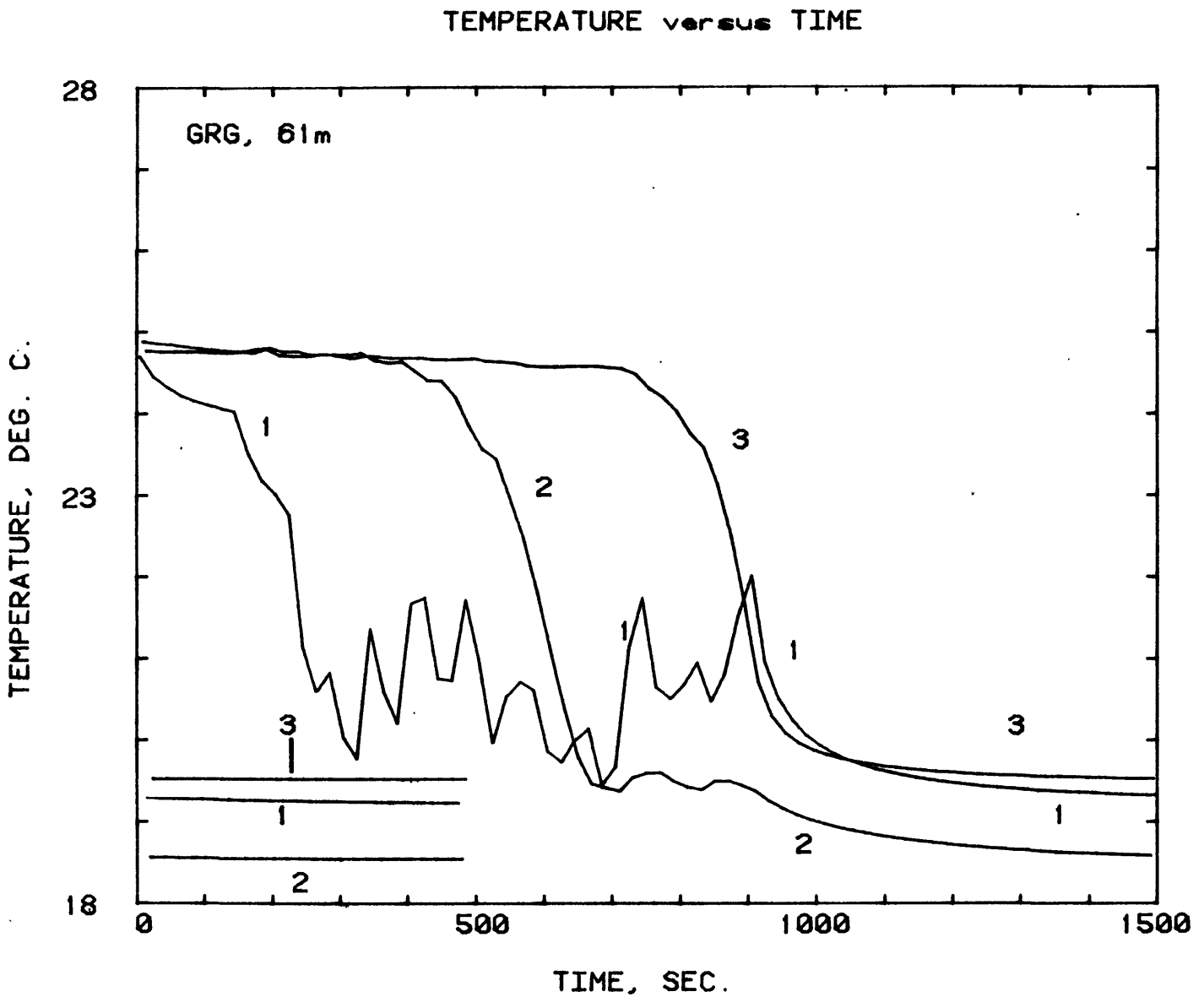

Figure 13. Penetration record for downhole probe run in Hole GRG, 61 meters. Lines at lower left are continuations of the original decay curves ($t_o \simeq 1600$ sec).

SUMMARY AND CONCLUSIONS

A downhole probe capable of precise determinations of formation temperature and thermal conductivity and rough estimates of the thermal gradient over one meter can be inserted through a drill bit into unconsolidated sediments, activated, and removed in the time normally taken for a coring run. Two or more penetrations of the probe provide a heat-flow determination comparable in accuracy to a conventional heat-flow measurement without the necessity of casing the hole or relogging it after completion of drilling. The heat-flow determination is made during the drilling process; thus, there is no time delay in obtaining data, no surface hazards associated with protruding casing, and no opportunity for unauthorized entry to boreholes in sensitive and/or competitive prospects. Because the hole need not be cased, grouted or visited repeatedly, the technique also is very cost-effective.

Useful information was obtained in all 29 runs in the present study, demonstrating the robustness and the reliability of the equipment. In one hole, data obtained with the downhole probe provided evidence that the drilling process locally altered the thermal regime by permitting vertical water movement even though the casing was grouted in.

Many prospectively important geothermal systems are located within or adjacent to the alluvial and lacustrine sedimentary formations of the western United States. Using the technique outlined in this report, it should be possible to obtain 4 or 5 probe runs per day to depths of

between 50 and 150 meters in these formations, thus allowing two high-quality heat-flow data or several reconnaissance heat-flow estimates per day. Even if the field conditions and program objectives call for casing the wells, the reliable determinations *in situ* of thermal conductivity and the "real time" estimates of heat flow make the downhole probe a valuable adjunct to the standard approach.

References

Bonham, H. F., 1969, Geology and mineral deposits of Washoe and Storey counties, Nevada: Nevada Bureau of Mines Bulletin 70, 140 p.

Bullard, E. C., 1954, The flow of heat through the floor of the Atlantic Ocean: Proceedings of the Royal Society of London, A, v. 222, p. 408-429.

Jaeger, J. C., 1958, The measurement of thermal conductivity and diffusivity with cylindrical probes: American Geophysical Union Transactions, v. 39, p. 708-710.

Keller, G. V., and Grose, L. T., 1978, Studies of a geothermal system in northwestern Nevada--Part 1: Colorado School of Mines Quarterly, v. 73, no. 3, 84 p.

Lachenbruch, A. H., 1957, A probe for measurement of thermal conductivity of frozen soils in place: American Geophysical Union Transactions, v. 38, p. 691-697.

Lachenbruch, A. H., and Brewer, M. C., 1959, Dissipation of the temperature effect of drilling a well in Arctic Alaska: U.S. Geological Survey Bulletin 1083-C, p. 73-109.

Langseth, M. G., 1965, Techniques of measuring heat flow through the ocean floor, in Lee, W. H. K., ed., Terrestrial Heat Flow: American Geophysical Union Geophysical Monograph, v. 8, p. 58-77.

Moses, T. H., Jr., Sass, J. H., and Wendt, W. E., 1979, The U.S. Geological Survey digital temperature-logging system: U.S. Geological Survey Open-File Report, in preparation.

Olmsted, F. H., Glancy, P. A., Harrill, J. R., Rush, F. E., and VanDenburgh, A. S., 1975, Preliminary hydrogeologic appraisal of selected hydrothermal systems in northern and central Nevada: U.S. Geological Survey Open-File Report 75-56, p. 128-147.

Von Herzen, R. P., and Maxwell, A. E., 1959, The measurement of thermal conductivity of deep sea sediments by a needle probe method: Journal of Geophysical Research, v. 64, p. 1557-1563.

Willden, R., 1964, Geology and mineral deposits of Humboldt County, Nevada: Nevada Bureau of Mines Bulletin 59, 154 p.

APPENDIX A

Temperatures, Gradients, and Thermal Conductivity

In this section, we present temperature and conductivity profiles for all of the holes in the Black Rock Desert in which downhole probe experiments were performed (Figure 1). At least two temperature profiles are given for each hole; one shortly after drilling, another 2 1/2 months or more later, and in some instances a third profile, at an intermediate time. The top of the cement column in the annulus between casing and borehole wall is easily identified by the positive "kick" in the earliest temperature profile (see e.g., Figure A-1 at ∿50 m). The individual temperatures determined from the lowermost thermistor (#1) are plotted as open circles on the diagrams. In the logging mode, temperatures were measured at intervals of 0.3 m (1 foot) (see Moses and others, 1979). The gradients shown are sliding averages over 3.05 meters (10 ft). Shown with the gradients are the harmonic mean conductivities for the probed intervals. Where cores were obtained, the means for cored and probed intervals are combined as a single value. For more details for a given figure number, see the corresponding table in Appendix B.

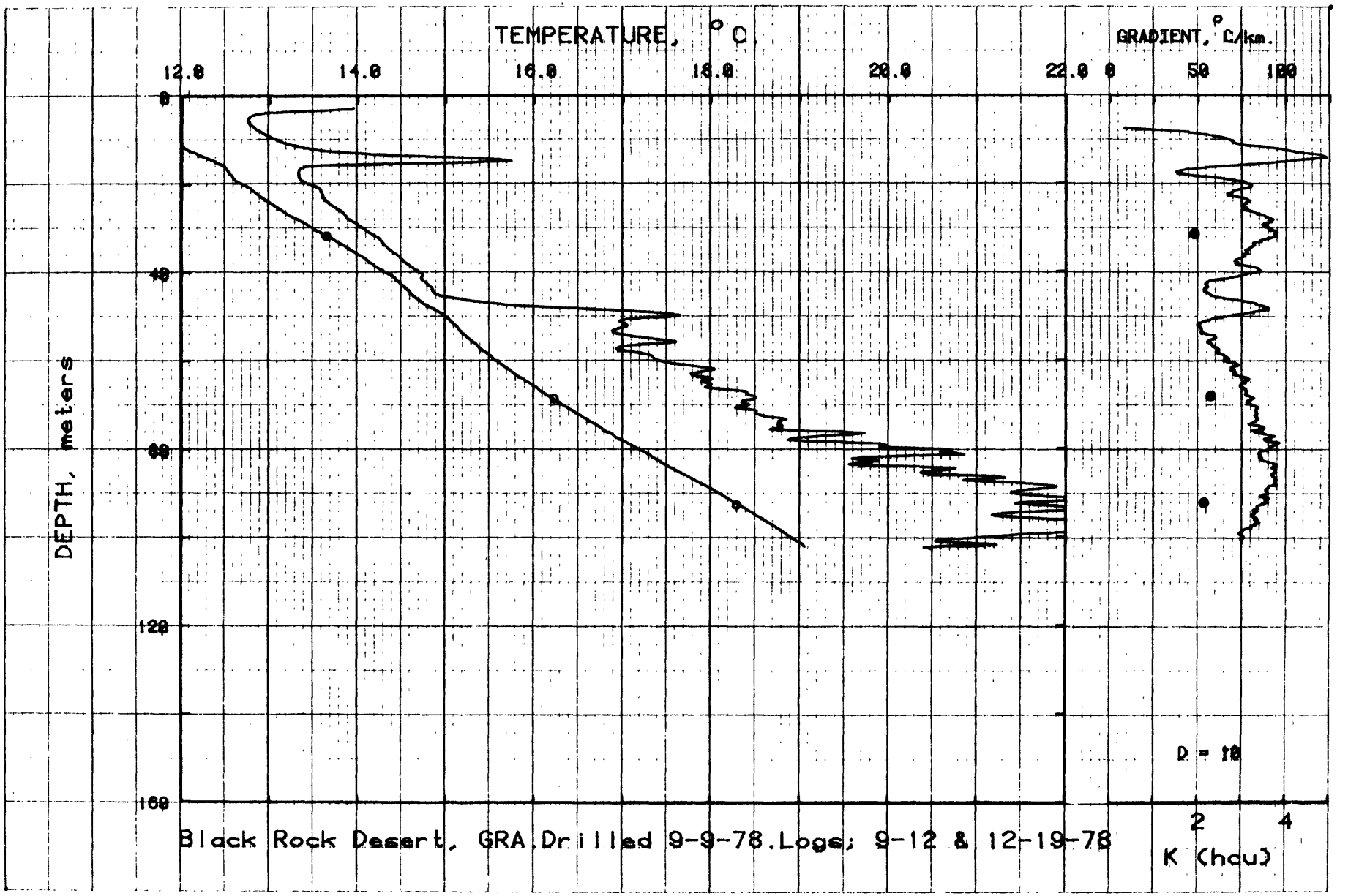

Figure A-1. Temperatures, gradients, and thermal conductivities, Hole GRA.

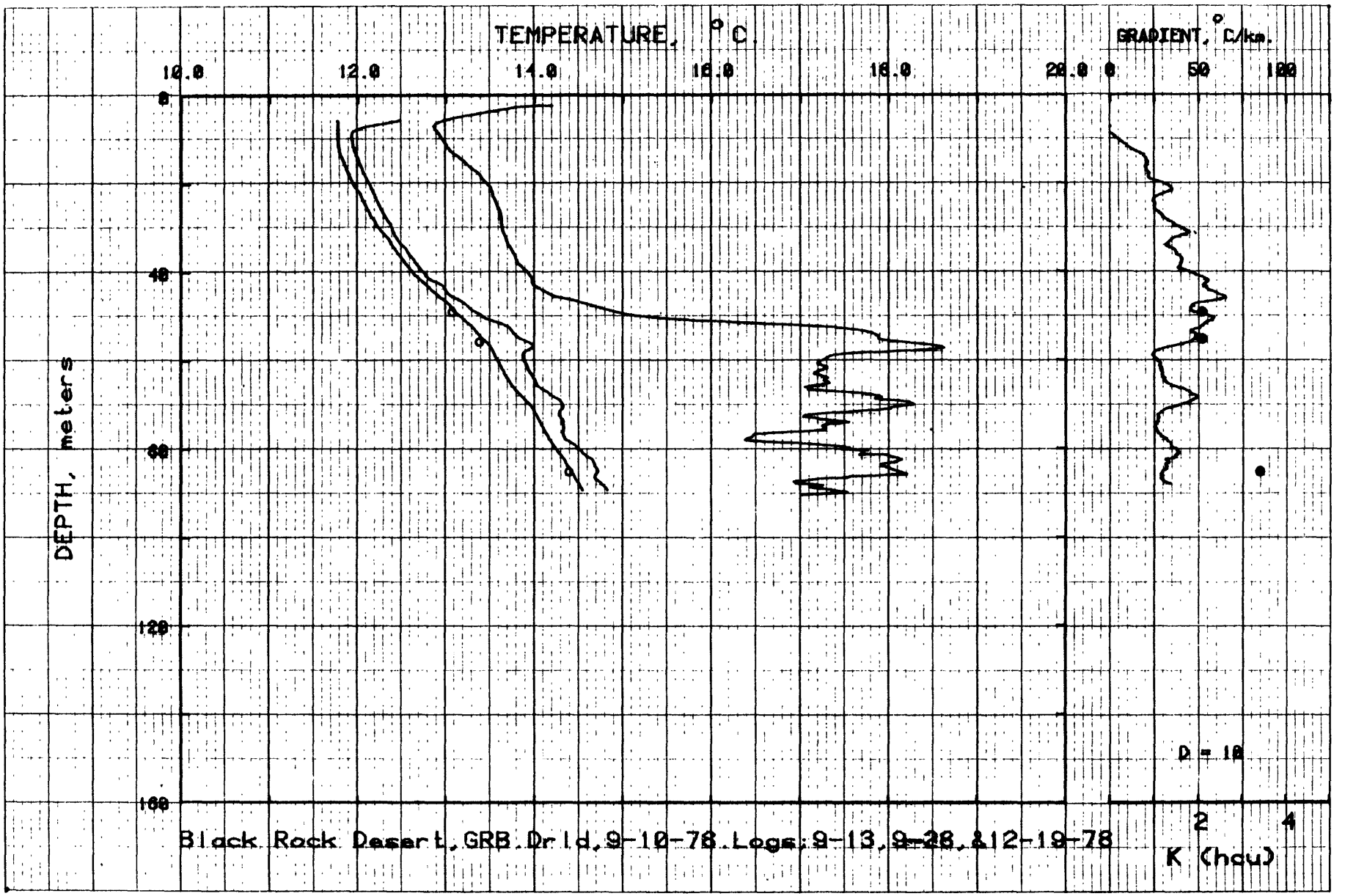

Figure A-2. Temperatures, gradients, and thermal conductivities, Hole GRB.

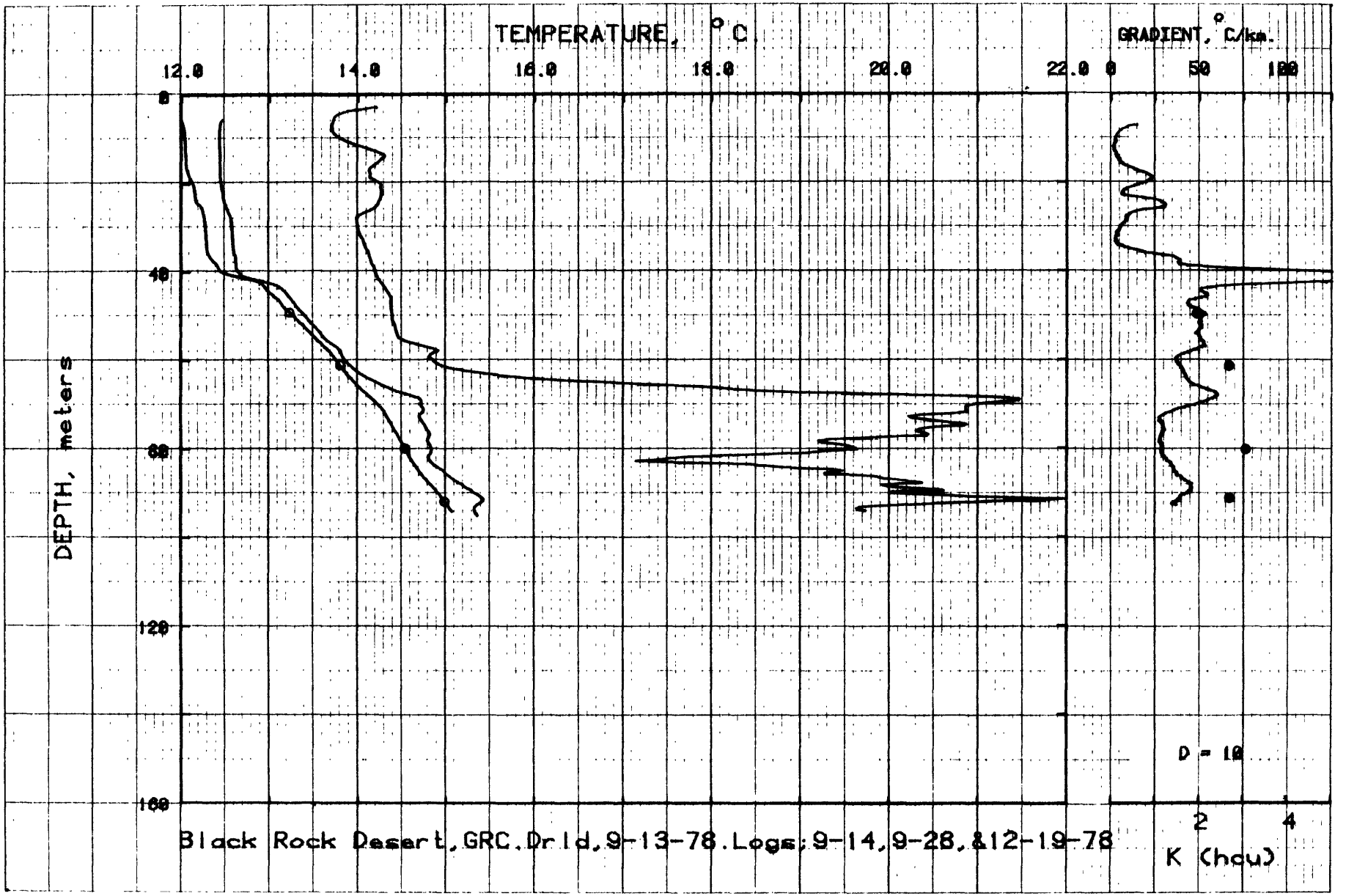

Figure A-3. Temperatures, gradients, and thermal conductivities, Hole GRC.

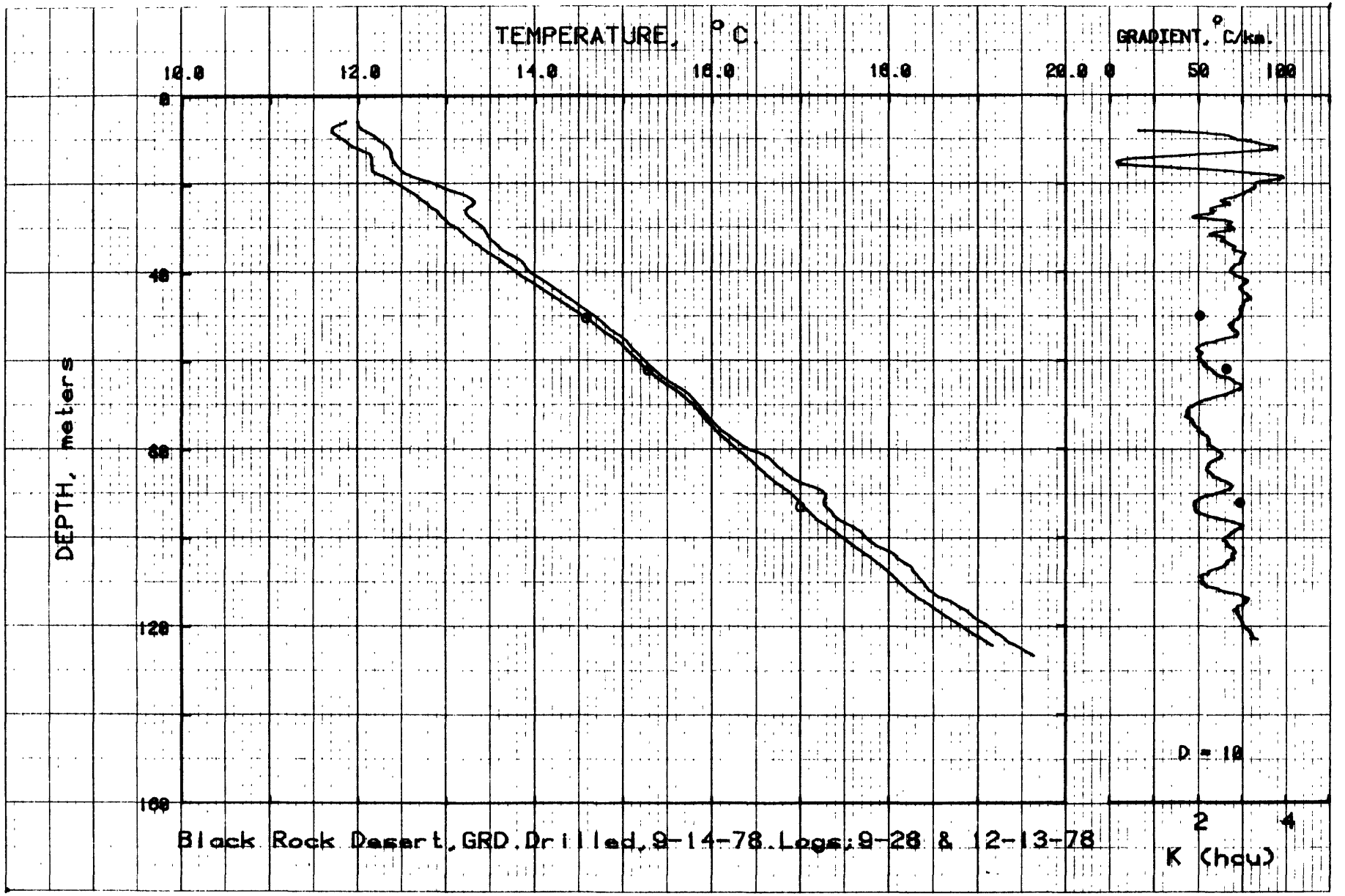

Figure A-4. Temperatures, gradients, and thermal conductivities, Hole GRD.

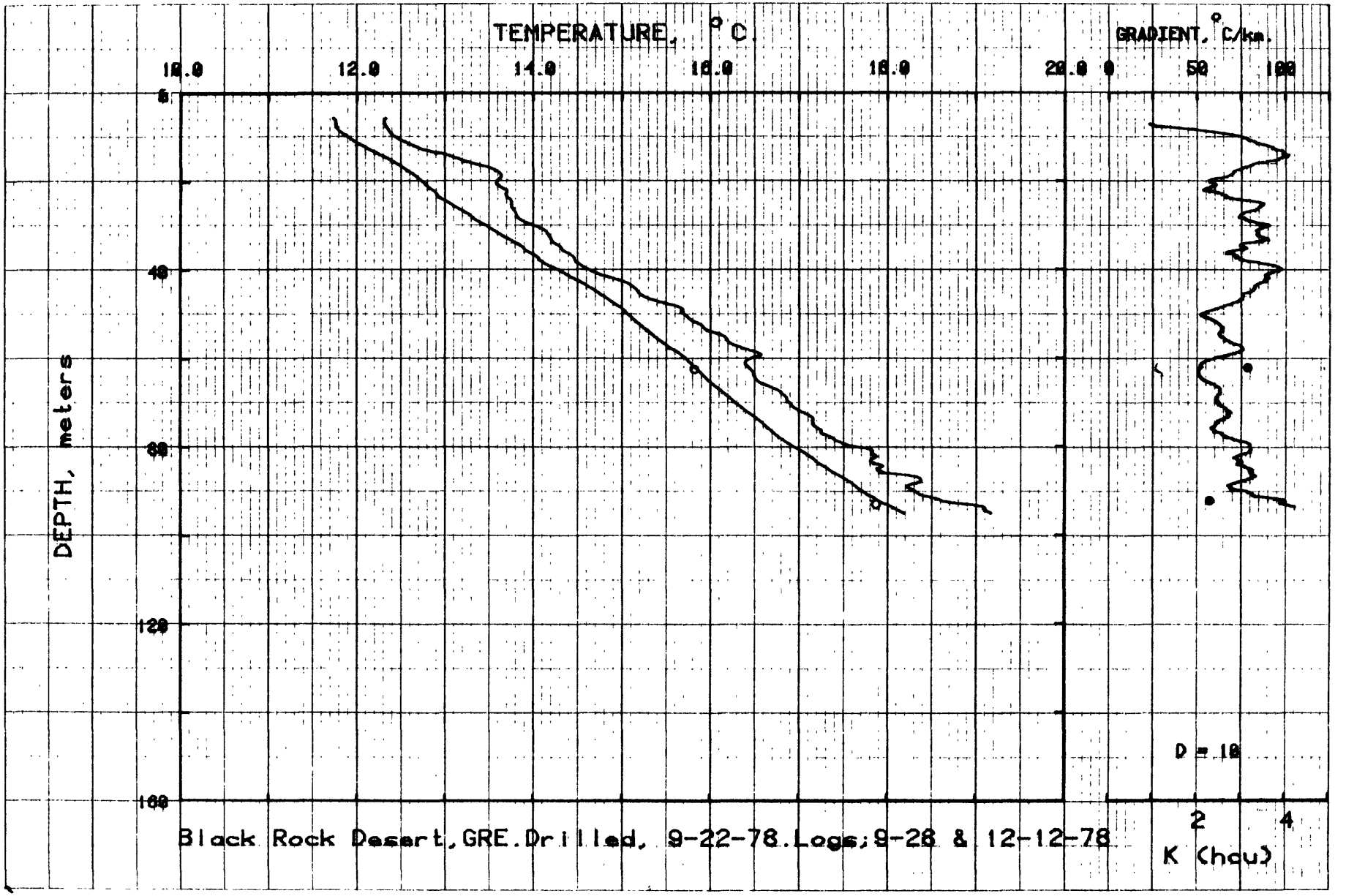

Figure A-5. Temperatures, gradients, and thermal conductivities, Hole GRE.

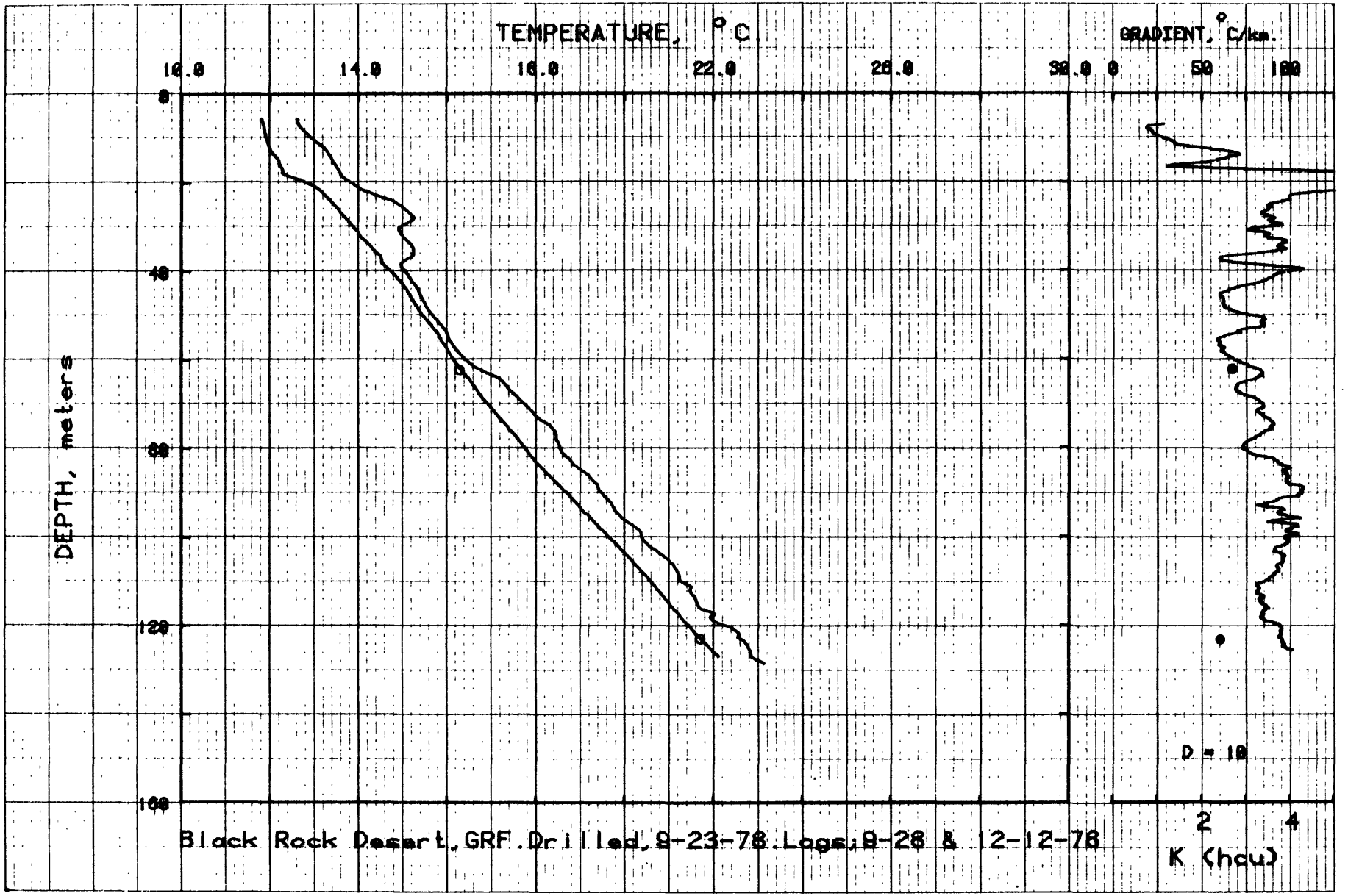

Figure A-6. Temperatures, gradients, and thermal conductivities, Hole GRF.

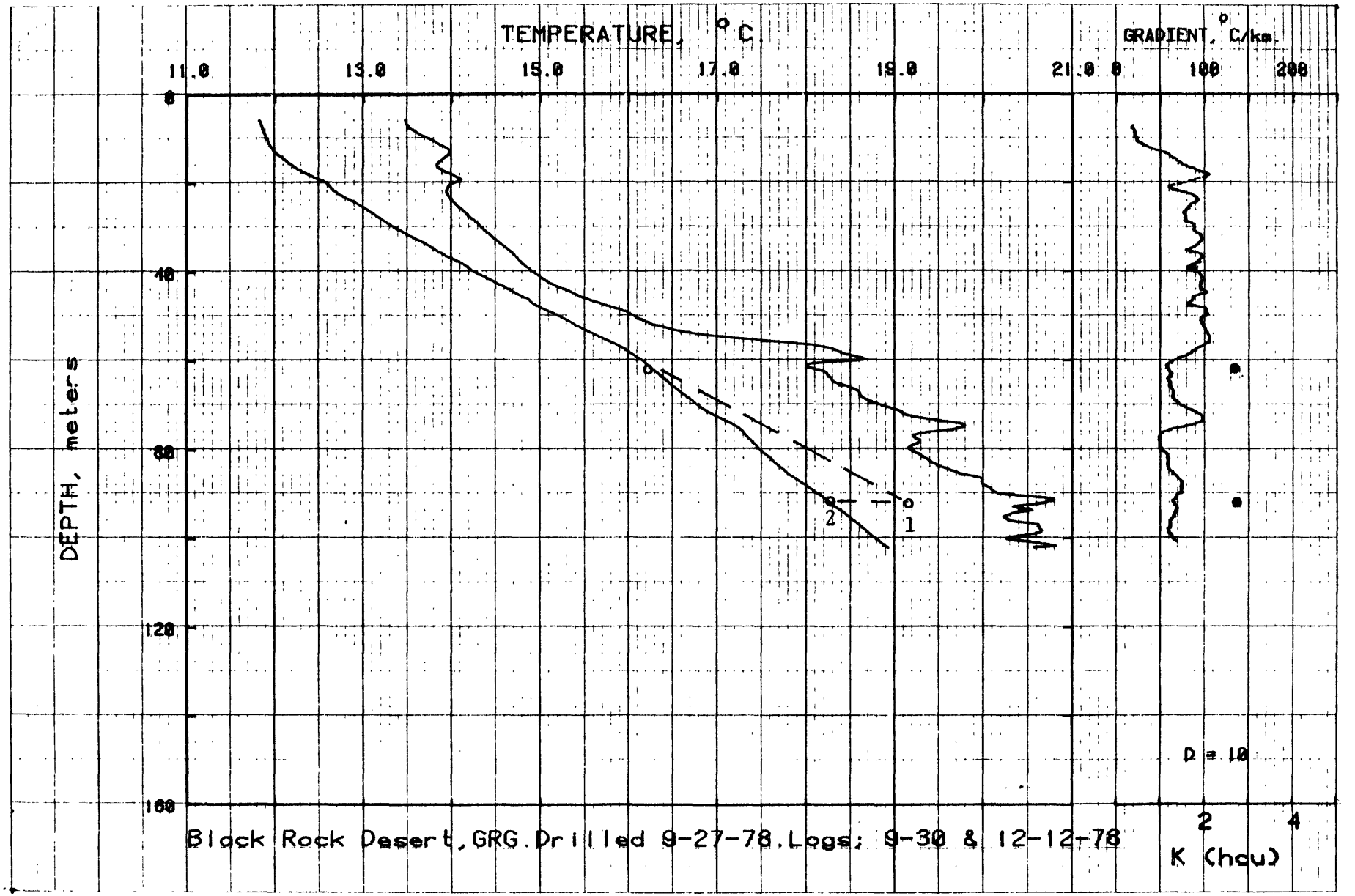

Figure A-7. Temperatures, gradients, and thermal conductivities, Hole GRG.

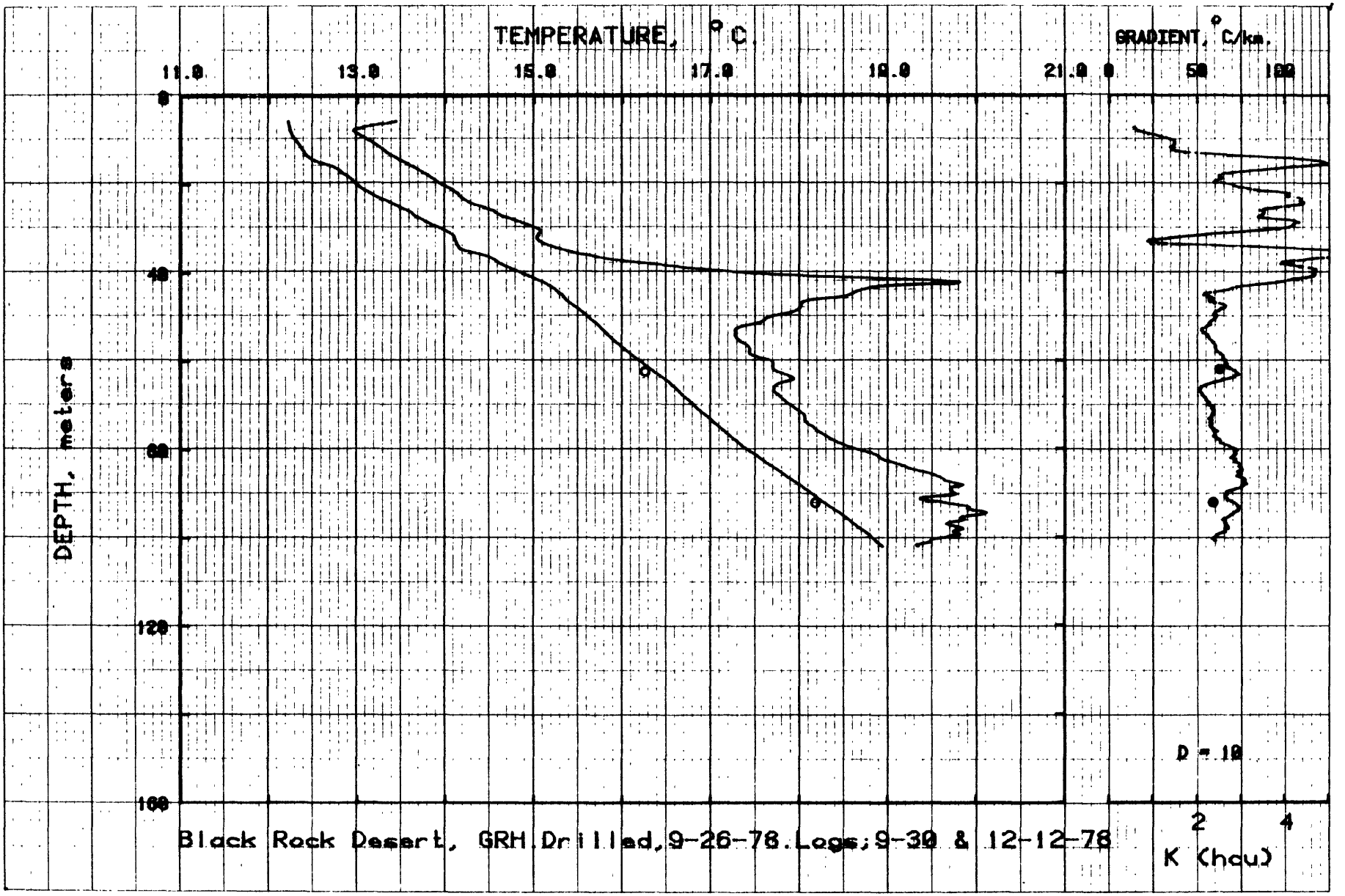

Figure A-8. Temperatures, gradients, and thermal conductivities, Hole GRH.

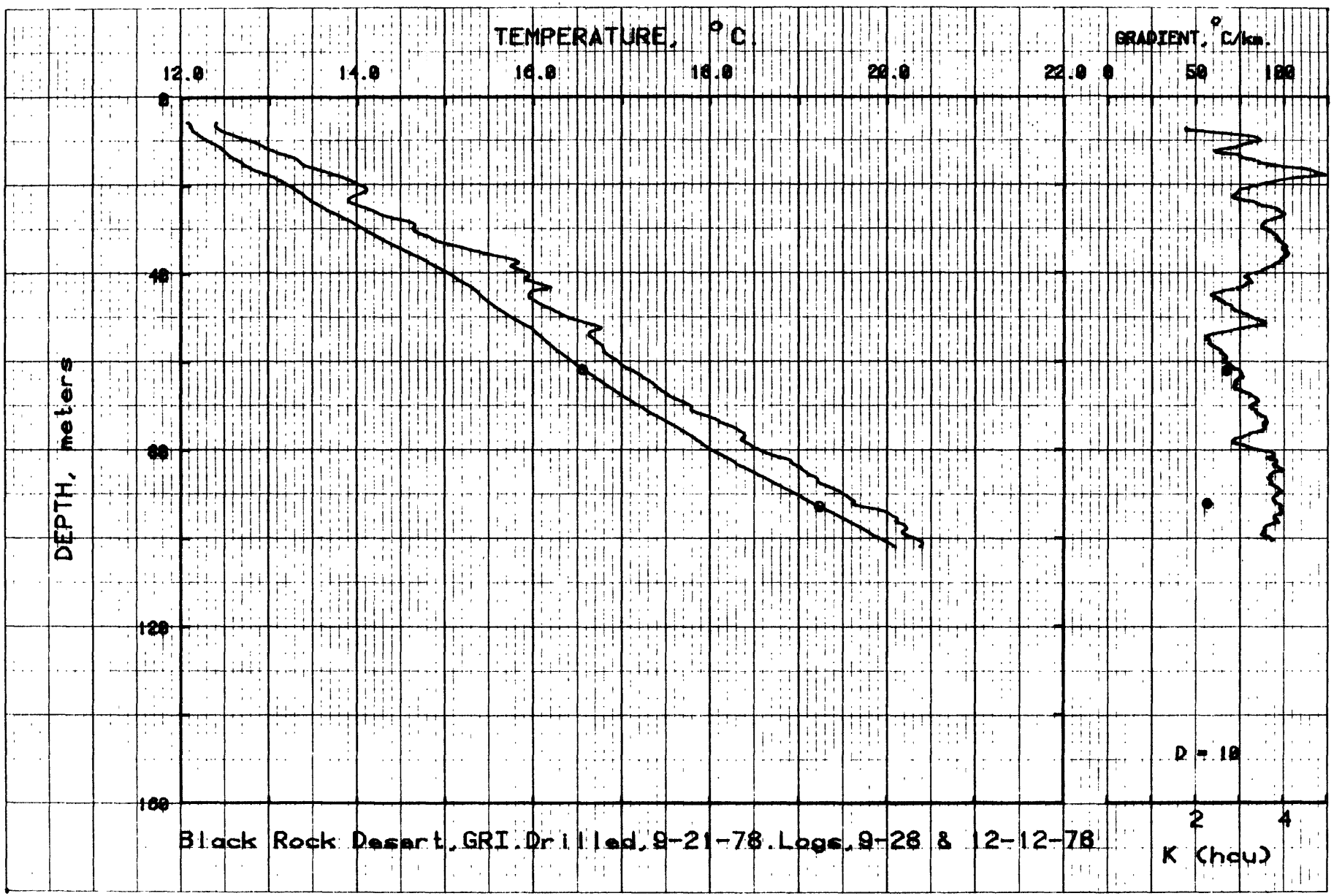

Figure A-9. Temperatures, gradients, and thermal conductivities, Hole GRI.

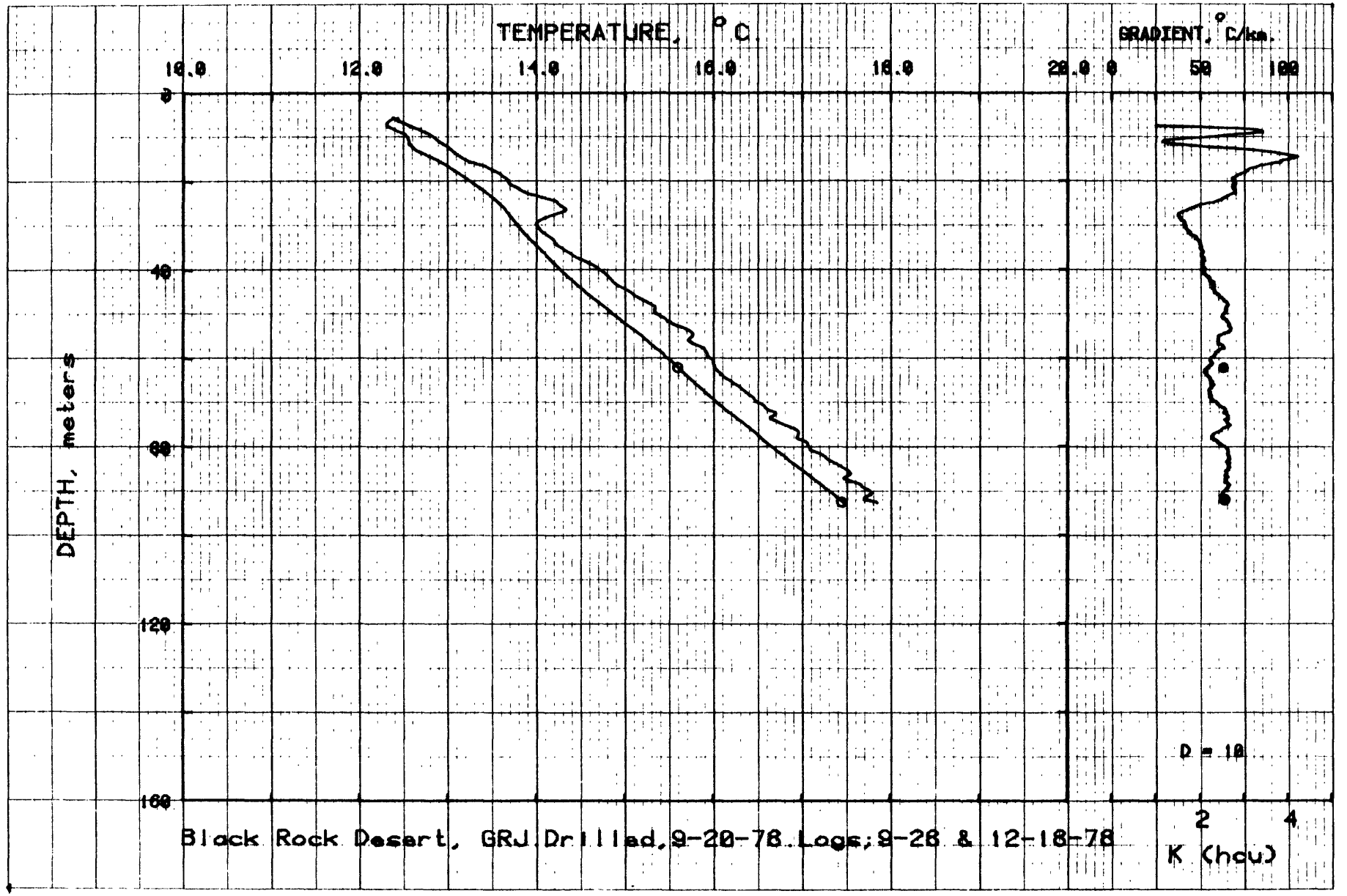

Figure A-10. Temperatures, gradients, and thermal conductivities, Hole GRJ.

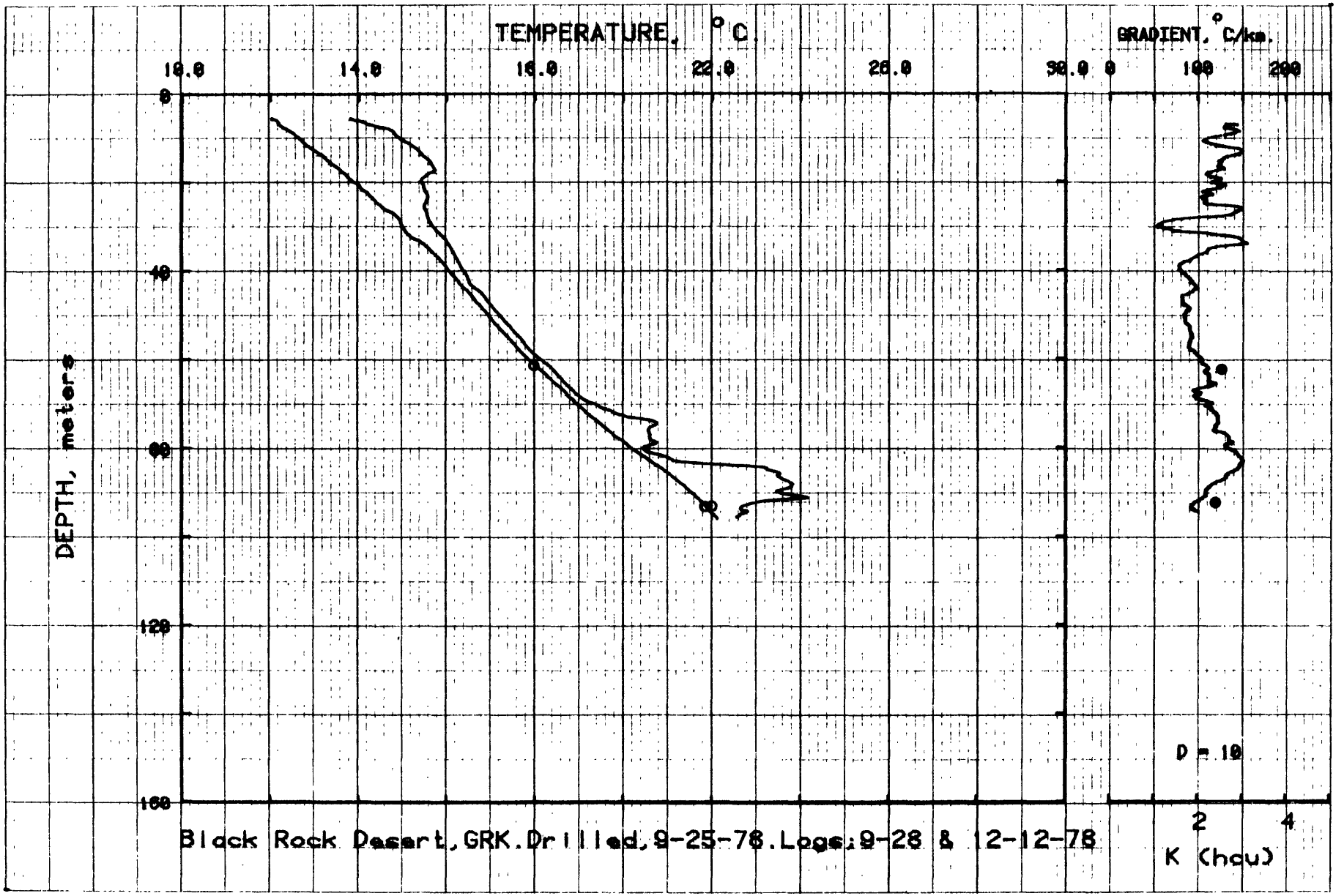

Figure A-11. Temperatures, gradients, and thermal conductivities, Hole GRK.

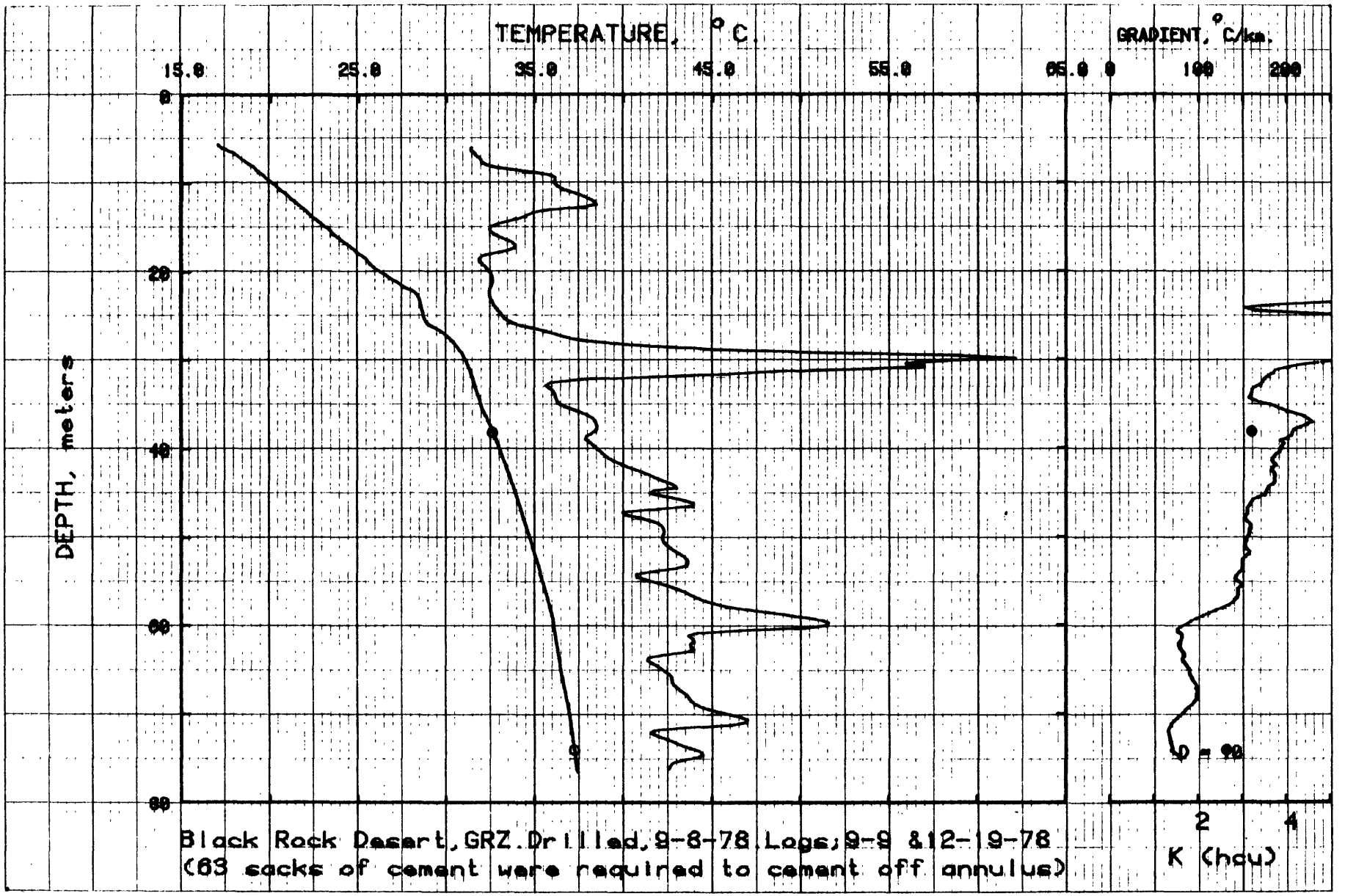

Figure A-12. Temperatures, gradients, and thermal conductivities, Hole GRZ.

APPENDIX B

Summaries of Downhole Experiments

Summaries of all downhole experiments are tabulated in this section. For each hole, we present a table showing the results from the downhole probe compared with conventional measurements. The first three columns give reference depths; the first, the approximate depth reached by the bit before the experiment began. The second column refers to the depths of the probe thermistors assuming that the bit depth is accurate. Actually, because of shifting reference levels on the rig relative to the ground surface, the accuracy of the bit-depth estimate is probably no better than $\pm$0.3 m. For penetrations (column three) of less than 1.15 m, only one or two depths are shown depending on how many thermistors actually penetrated the formation beyond the bit. Temperatures obtained from linear extrapolation of the temperature versus 1/time curves (see Figures 5 and 6) are compared with those obtained from the most recent temperature logs in columns 4 and 5 (see also the corresponding temperature curves in Appendix A). The closeness of the agreement should be judged in the light of the $\pm$0.3 m uncertainty in bit location already mentioned, a similar uncertainty in reference level for the temperature log, and an uncertainty of $\pm$0.01°C in the value of temperature obtained using the downhole probe. At a temperature gradient of 100°C/km, an unfavorable combination of these factors can result in a discrepancy of nearly 0.1°C between the two temperature columns. In fact, the discrepancy is

usually much less than this except where there was obviously a disturbance caused by the invasion of drilling fluid.

The comparison between the gradient columns is not so much affected by difficulties in establishing a surface reference datum. (The "Log" gradient was determined by a least-squares fit to six temperature readings from the most recent log over the 1.5 m interval directly below the bit.) The main problem here is the insensitivity of the system. Since each thermistor is only calibrated (relative to the other two) to $\pm$0.01°C, we have a maximum possible error of $\pm$40°C/km over 0.5 m or $\pm$20°C/km over a meter. Although this is too coarse a determination for the usual range of regional background heat flows, it provides sufficient sensitivity for outlining anomalies of the magnitude (say 100 to 300°C/km) we might expect in unconsolidated sediments in an area of economic interest for geothermal exploration. In this context, the agreement in the gradient columns is quite satisfactory. Furthermore, accuracy can be improved, and confidence increased by making two or more probe runs 10 or more meters apart as we have done in every case. When we have full penetration at two locations giving one-meter heat flows which agree with that estimated over several tens of meters (see e.g., summary for GRF, Table B-6), then we have sufficient redundancy to give us a value of stature comparable to that of a conventional heat-flow measurement where we have taken two or more separate cores.

TABLE B-1. Summary of downhole probe experiments, Hole GRA, Black Rock Desert, Nevada

Depth, m		Penetration	Temperature °C		Gradient °C/km		Conductivity (HCU)		Heat flow (HFU)	
Bit	Thermistor	m	Probe	Log	Probe	Log	Probe	Core	Probe	Log
30.5		1.65								
	31.0		13.596	13.582	64		1.96	1.83		
	31.5		13.628	13.620	88		2.03	1.82		
	32.0		13.672	13.667			2.03	1.82		
					76	85	2.01	1.82	1.54	1.55
67.10		1.65								
	67.6		16.126	16.125	50		2.30	2.31		
	68.1		16.151	16.168	98		2.24	2.24		
	68.6		16.200	16.205			2.35	2.30		
					74	80	2.30	2.28	1.70	1.82
91.44		1.40								
	91.7		18.257	18.229	48*		2.23	2.10		
	92.2		18.281	18.226	15*		2.23	2.21		
	92.7		18.288	18.307			2.21	2.08		
					32*	78	2.22	2.13	(0.7)*	1.66
								Mean	1.62	1.68
Interval heat flows										
32-69m					66.6	69.3	2.15	2.05	1.43	1.42
69-93					86.6	87.2	2.26	2.20	1.96	1.92
32-93					76.1	76.4	2.18	2.08	1.66	1.59
Least-squares intervals										
20-40m					82.8±0.4		1.91±0.1		1.58±0.09	
61-103					85.8±0.2		2.23±0.04		1.91±0.04	
30-103					76.2±0.3		2.11±0.08		1.61±0.07	
							Best value		1.7 ±0.2	

*Electrical noise in record. Excluded from means.

TABLE B-2. Summary of downhole probe experiments, Hole GRB, Black Rock Desert, Nevada

Depth, m		Penetration	Temperature °C		Gradient °C/km		Conductivity (HCU)		Heat flow (HFU)	
Bit	Thermistor	m	Probe	Log	Probe	Log	Probe	Core	Probe	Log
48.8		0.76								
	48.9						2.08			
	49.4		13.081	13.124			2.02			
							2.05			
54.9		1.17								
	55.4		13.379	13.436	26	50	2.19	1.98	0.6	1.0
	55.9		13.392	13.463			2.14	2.03		
							2.16	2.00		
85.0		0.46								
	85.3		14.390	14.427			3.44	2.5-3.5		
Interval heat flows										
49-56m					47.8	52.1	2.10	2.00	1.00	1.04
56-85					36.5	36.3	2.50	2.50	0.91	0.91
							Best value		1.0 ± 0.1	

TABLE B-3. Summary of downhole probe experiments, Hole GRC, Black Rock Desert, Nevada

Depth, m		Penetration	Temperature °C		Gradient °C/km		Conductivity (HCU)		Heat flow (HFU)	
Bit	Thermistor	m	Probe	Log	Probe	Log	Probe	Core	Probe	Log
48.77		1.02								
	49.13		13.214	13.230	52	55	2.00	2.06		
	49.63		13.240	13.257			1.88	1.96		
							1.94	2.01	1.01	1.11
60.96		0.64								
	61.45		13.813	13.811		41	2.72	2.63		1.08
79.25		0.86								
	79.45		14.511	14.526	45	28	3.22	2.88		
								2.90		
	79.95		14.534	14.540			3.26	2.83		
							3.24	2.87	1.46	0.80
91.44		1.0								
	91.80		15.040*	14.985	-84*	35	2.62	2.67		
								2.41		
	92.30		14.996	15.001			2.91	2.85		0.92
							2.77	2.64		
								Mean	1.24	0.98
Interval heat flows										
50-61m					48.5	46.9	2.33	2.32	1.13	1.09
61-80					39.0	39.4	2.98	2.75	1.16	1.08
80-92					37.4	37.3	3.01	2.76	1.12	1.03
50-92					41.2	40.9	2.58	2.49	1.06	1.02
								Means	1.12	1.06
Least-squares intervals										
42-71m					47.5±0.2		2.27±0.30		1.08±0.10	
73-94					34.9±0.4		2.86±0.24		1.0 ±0.1	
50-94					40.0±0.3		2.53±0.17		1.01±0.08	
							Best value		1.0 ±0.1	

*Circulation lost before test. This test probably affected by invasion of drilling fluid.

TABLE B-4. Summary of downhole probe experiments, Hole GRD, Black Rock Desert, Nevada

Depth, m		Penetration	Temperature °C		Gradient °C/km		Conductivity (HCU)		Heat flow (HFU)	
Bit	Thermistor	m	Probe	Log	Probe	Log	Probe	Core	Probe	Log
48.7		1.65								
	49.27		14.505	14.497	82		2.02			
	49.77		14.546	14.536			2.10			
	50.27		14.582	14.574	72		2.05			
					77	74.5	2.05		1.58	1.53
60.96		1.52								
	61.33		15.250	15.236	48		2.52			
	61.83		15.274	15.264	44		2.74			
	62.33		15.296	15.296						
					46	59	2.65		1.22	1.56
91.44		1.65								
	91.94		16.955	16.992	41		2.60			
	92.44		16.976	17.016			3.15			
	92.94		16.997	17.039	43		3.16			
					42	47	2.94		1.24	1.38
								Mean	1.35	1.49
Interval heat flows										
50-62m					52.9	59.9	2.35		1.39	1.41
62-93					55.6	56.9	2.80		1.56	1.59
50-93					56.6	57.8	2.50		1.42	1.44
								Mean	1.46	1.48
Least-squares intervals										
30-55m					72.9±0.2		2.05±0.02		1.49±0.02	
55-96					56.0±0.1		2.80±0.11		1.57±0.06	
								Best value	1.4±0.1	

TABLE B-5. Summary of downhole probe experiments, Hole GRE, Black Rock Desert, Nevada

Depth, m		Penetration	Temperature °C		Gradient °C/km		Conductivity (HCU)		Heat flow (HFU)	
Bit	Thermistor	m	Probe	Log	Probe	Log	Probe	Core	Probe	Log
61		1.65								
	61.5		15.765	15.784			2.96			
					43					
	62.0		15.786	15.810			3.20			
					69					
	62.5		15.821	15.851			3.32			
					56	52	3.16		1.77	1.64
91.44		1.65								
	91.94		17.885	17.872			2.36			
					-100					
	92.44		17.829	17.909			2.21			
					66					
	92.94		17.862	17.967			2.28			
						83	2.28			1.89
Interval heat flow										
62-93m					67.1	69.5	2.72		1.82	1.89
Least-squares interval										
60-93m						68.1±0.4	2.65±0.19			1.80±0.14
							Best value			1.8±0.1

TABLE B-6. Summary of downhole probe experiments, Hole GRF, Black Rock Desert, Nevada

Depth, m		Penetration	Temperature °C		Gradient °C/km		Conductivity (HCU)		Heat flow (HFU)	
Bit	Thermistor	m	Probe	Log	Probe	Log	Probe	Core	Probe	Log
61		1.65								
	61.5		16.241	16.258	62		2.69			
	62.0		16.272	16.303	98		2.70			
	62.5		16.321	16.332						
					80	76	2.70		2.16	2.05
121.9		1.65								
	122.4		21.627	21.656	113		2.41			
	122.9		21.665	21.703	76		2.39			
	123.4		21.721	21.752			2.44			
					95	95	2.41		2.29	2.29
							Mean		2.23	2.17
Interval heat flow										
62-123					88.7	89.0	2.55		2.26	2.27
Least-squares intervals										
42-83					74.4±0.3		2.70±0.01		2.01±0.02	
84-126					92.5±0.2		2.41±0.02		2.23±0.02	
							Best value		2.2±0.1	

TABLE B-7. Summary of downhole probe experiments, Hole GRC, Black Rock Desert, Nevada

Depth, m		Penetration	Temperature °C		Gradient °C/km		Conductivity (HCU)		Heat flow (HFU)	
Bit	Thermistor	m	Probe	Log	Probe	Log	Probe	Core	Probe	Log
61		1.65								
	61.5		16.162	16.241			2.90			
					26					
	62.0		16.175	16.272			2.85			
					75					
	62.5		16.213	16.302			2.45			
					51	58	2.72		1.39	1.58
91.44		1.16								
	92.0		18.281	18.266			2.63			
					1800					
	92.5		19.167*	18.300			2.85			
					1800*	65	2.74		~49*	1.78
Interval heat flows										
62-92					70.2	66.5	2.73		1.92	1.82
62.5-92.5					98.5	66.6	2.73		2.69	1.82
Least-squares intervals										
30-56						93.5±0.2	2.0?			1.87
							2.73?			2.55
60-102						66.1±0.2	2.73±0.02		1.80±0.02	
							Best value			2.6

*See Figure A-7 and discussion in main body of report.

TABLE B-8. Summary of downhole probe experiments, Hole GRH, Black Rock Desert, Nevada

Depth, m		Penetration	Temperature °C		Gradient °C/km		Conductivity (HCU)		Heat flow (HFU)	
Bit	Thermistor	m	Probe	Log	Probe	Log	Probe	Core	Probe	Log
61		1.65								
	61.5		16.206	16.294			2.32			
					48					
	62.0		16.230	16.326			2.61			
					80					
	62.5		16.270	16.360			2.62			
					64	66	2.51		1.61	1.66
91.44		0.65								
	91.94		18.190	18.269			2.35			
Interval heat flow										
62.5-91.9					65.2	64.8	2.47		1.61	1.60
Least-squares interval										
45-101						63.8±0.2		2.47±0.08		1.58±0.06
							Best value			1.6±0.1

TABLE B-9. Summary of downhole probe experiments, Hole GRI, Black Rock Desert, Nevada

Depth, m		Penetration	Temperature °C		Gradient °C/km		Conductivity (HCU)		Heat flow (HFU)	
Bit	Thermistor	m	Probe	Log	Probe	Log	Probe	Core	Probe	Log
61.0		1.2								
	61.5		16.514	16.531			2.86			
	62.0		16.536	16.569			2.59			
						73	2.72			1.99
91.44		1.52								
	91.8		19.151	19.126	117		2.35			
	92.3		19.209	19.171			2.19			
	92.8		19.240	19.223	61		2.21			
					89	96	2.25		2.00	2.16
							Mean		1.61	2.08
Interval heat flow										
62-93					87.8	86.2	2.48		2.18	2.14
Least-squares intervals										
40-80					73.3±0.3		2.72±0.12		1.99±0.1	
80-102					94.8±0.1		2.25±0.05		2.13±0.05	
							Best value		2.1±0.1	

TABLE B-10. Summary of downhole probe experiment, Hole GRJ, Black Rock Desert, Nevada

Depth, m		Penetration	Temperature °C		Gradient °C/km		Conductivity (HCU)		Heat flow (HFU)	
Bit	Thermistor	m	Probe	Log	Probe	Log	Probe	Core	Probe	Log
61.0		1.50								
	61.35		15.539	15.559	47		2.46			
	61.85		15.563	15.587	50		2.53			
	62.35		15.588	15.612			2.61			
					49	55	2.53		1.24	1.39
91.44		1.20								
	92.0		17.412	17.427	54		2.50			
	92.5		17.439	17.460			2.62			
					54	62	2.56		1.38	1.59
							Mean		1.31	1.49
Interval heat flow										
62-92					61.4	61.3	2.54		1.56	1.56
Least-squares interval										
40-93					60.5±0.1		2.54±0.03		1.54±0.02	
							Best value		1.55±0.1	

TABLE B-11. Summary of downhole probe experiments, Hole GRK, Black Rock Desert, Nevada

Depth, m		Penetration	Temperature °C		Gradient °C/km		Conductivity (HCU)		Heat flow (HFU)	
Bit	Thermistor	m	Probe	Log	Probe	Log	Probe	Core	Probe	Log
61		0.8								
	61.11		17.954	17.969			2.49			
					82					
	61.61		17.995	18.019			2.60			
					82	105	2.55		2.09	2.68
91.44		1.65								
	91.94		21.785	21.729			2.26			
					98					
	92.44		21.834	21.778			2.39			
					311*					
	92.94		21.990*	21.829			2.51			
					205*	98	2.39		4.90*	2.34
Interval heat flows										
62-93					127.5	121.6	2.47		3.15	3.00
61-92					123.8	121.6	2.47		3.06	3.00
							Mean		3.1	3.0
Least-squares intervals										
40-60						89.3±0.2	2.55±0.05			2.28±
60-80						114.2±0.6	2.39±0.1			2.73±
							Best value			2.8±0.3

*Lost circulation between 61 and 91 meters. Formation appears to have been invaded by drilling fluid at the level of thermistor 1 (92.94 m).

TABLE B-12. Summary of downhole probe experiments, Hole GRZ, Black Rock Desert, Nevada

Depth, m		Penetration	Temperature °C		Gradient °C/km		Conductivity (HCU)		Heat flow (HFU)	
Bit	Thermistor	m	Probe	Log	Probe	Log	Probe	Core	Probe	Log
36.6		1.65								
	37.1		32.445	32.390	225		2.23	2.16		
	37.6		32.500	32.557			2.26	2.20		
	38.1		32.643	32.603	170		2.20	2.08		
					198	213	2.23	2.15	4.42	4.58
73.15		0.90						2.30		
	73.4		37.194	37.197	71		2.41	2.58		
	73.9		37.230	37.236			2.84	3.30 2.25		
					71	73	2.63	2.61	1.87	1.90
Interval heat flow										
38-74					128.1	129.4	2.43	2.38	3.11	3.08
Least-squares heat flow										
7-22						623±3		2.2±0.1		13.7±0.7*

*Shallow conductive cap overlying a thermal regime dominated by upward convection (see Figure B-12).

APPENDIX C

Mechanical Construction of Downhole Probe

The probe is essentially a 2.13 meter length of heat-treated 52100 grade steel, 6.4 mm o.d. and 3.2 mm i.d. Figure C-1 illustrates the main features and dimensions of the probe. A loop of heater wire and four thermistor leads, all mutually insulated and enclosed in heat shrinkable tubing are placed in the steel tube, and the voids are filled with molten woods metal.

The woods metal expands slightly on freezing, thereby facilitating thermal contact among heater, thermistors, and probe wall. The switching instrumentation (described in Appendix D) is attached at the top of the probe, and the entire probe is mated to the 3/16 inch (4.8 mm) o.d. four-conductor armored logging cable by means of a standard Gearhart-Owen cablehead. A short, smooth-walled 35 mm i.d. drill collar immediately above the bit acts as a cylinder for the piston on the driving mechanism (Figure C-2). The "grabber" (Figure C-3 and Plates I through III) consists of a series of ball bearings which roll up a ramped sleeve and compress the outer wall of the probe. For moderate pressures (up to 500 or 600 psi on the piston), the deformation is elastic, but at higher driving pressures, circular "dimples" are left on the probe wall. As the driving pressures approach the strength of the probe material, the dimples take on a teardrop shape (Plates I, II, and III). When the pressure is released, the grabber balls are free to move up the probe

under the force of the return spring so that when pressure is again applied, another increment of the probe can be pushed through the bit. The length of the stroke can be varied by using different lengths of return springs. In practice, the most efficient stroke length was found to be 8 to 10 cm. Shorter springs resulted in long times being required for penetration. Longer springs tended to buckle sideways and bind against the wall of the cylinder.

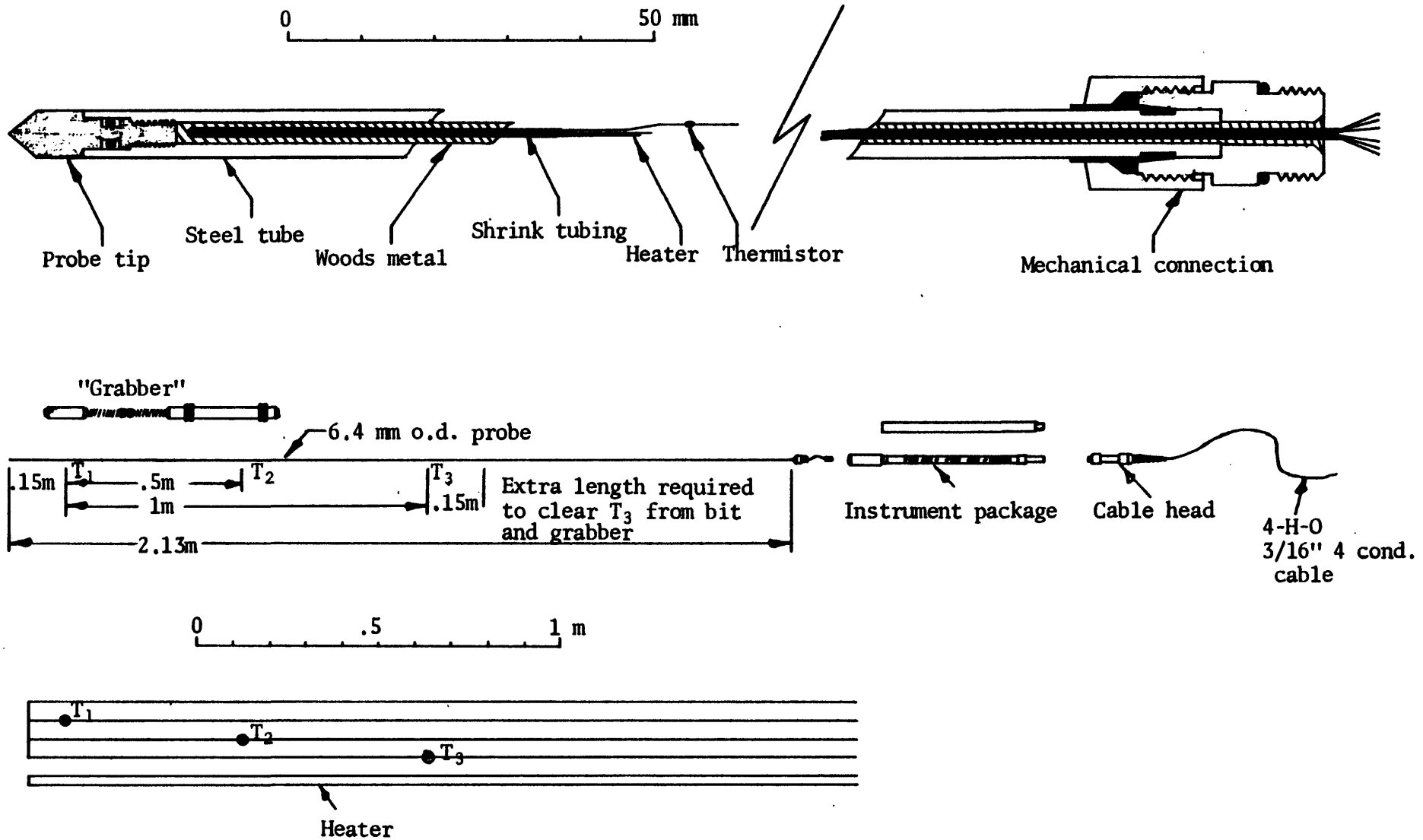

Figure C-1. Breakaway and schematic of downhole probe. a) Details of probe construction; b) Scale drawing showing relative dimensions of components; c) Wiring schematic for thermistors (T_1, T_2, and T_3) and heater.

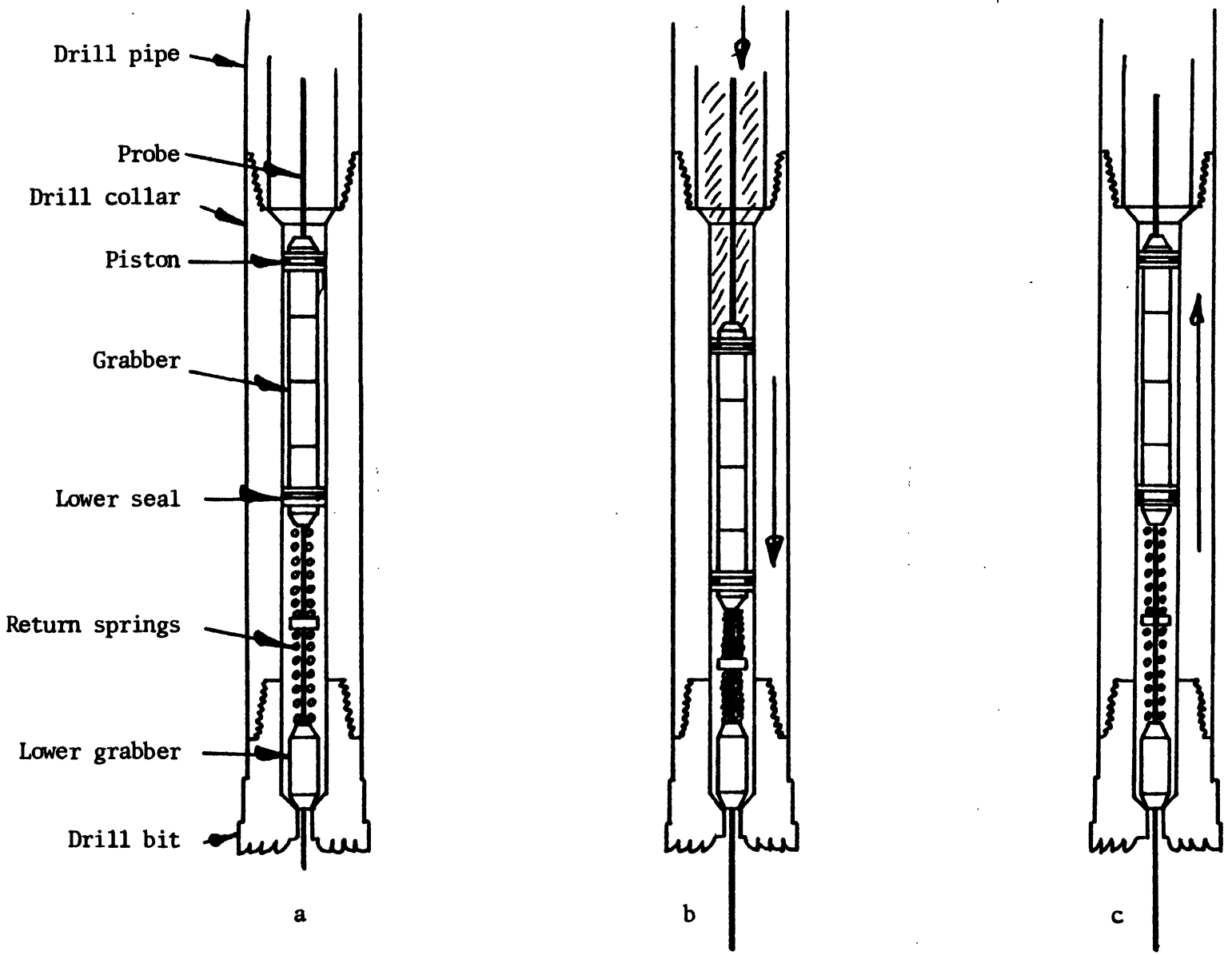

Figure C-2. Diagram illustrating a complete cycle of the probe driving mechanism. a) Probe at rest prior to beginning of penetration; b) ∿10 cm downstroke (up to 2000 psi [∿14000 kPa] may be applied to fluid column without damage to probe); c) return stroke - upon release of pressure, springs return grabber to upper part of piston.

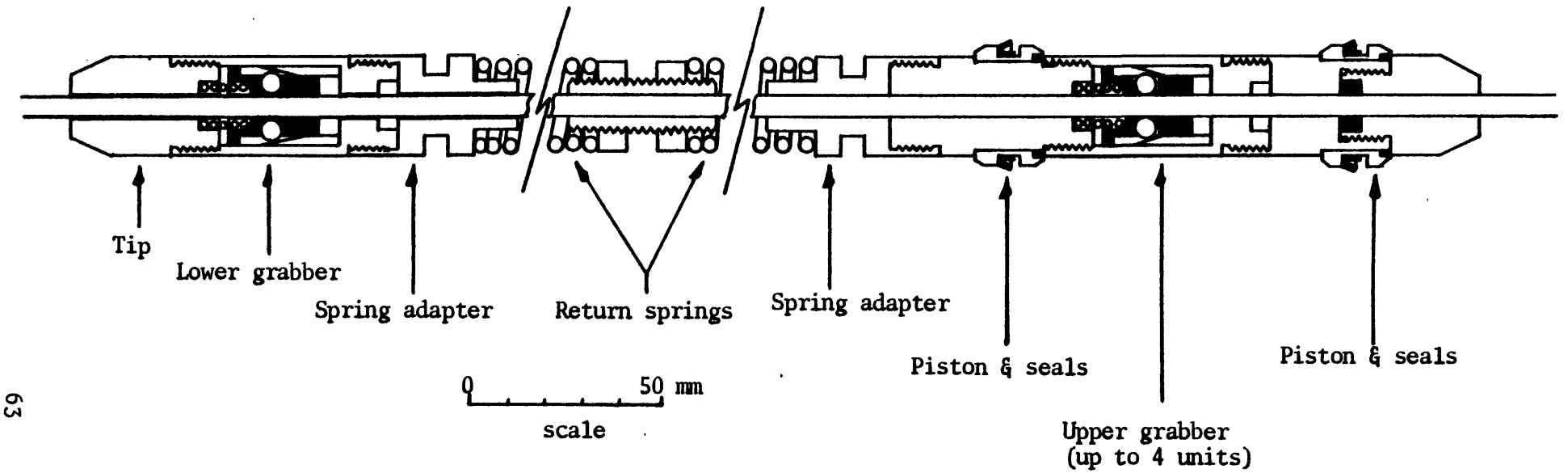

Figure C-3. Detailed diagram of probe-driving mechanism.

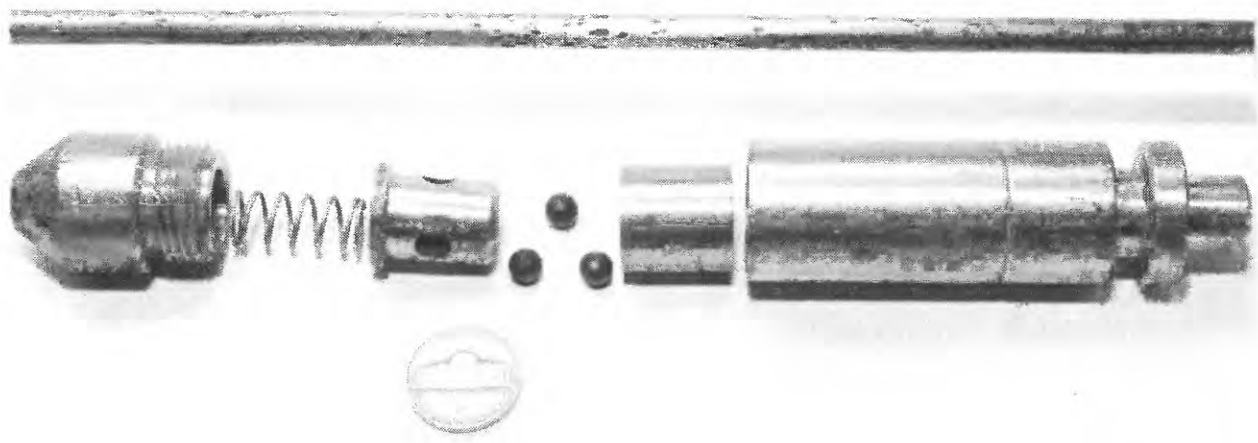

Plate I. Components of one "grabber"
(see drawing, Figure C-3)
and a section of a probe with 20 runs
showing dimples made by "grabber" balls.

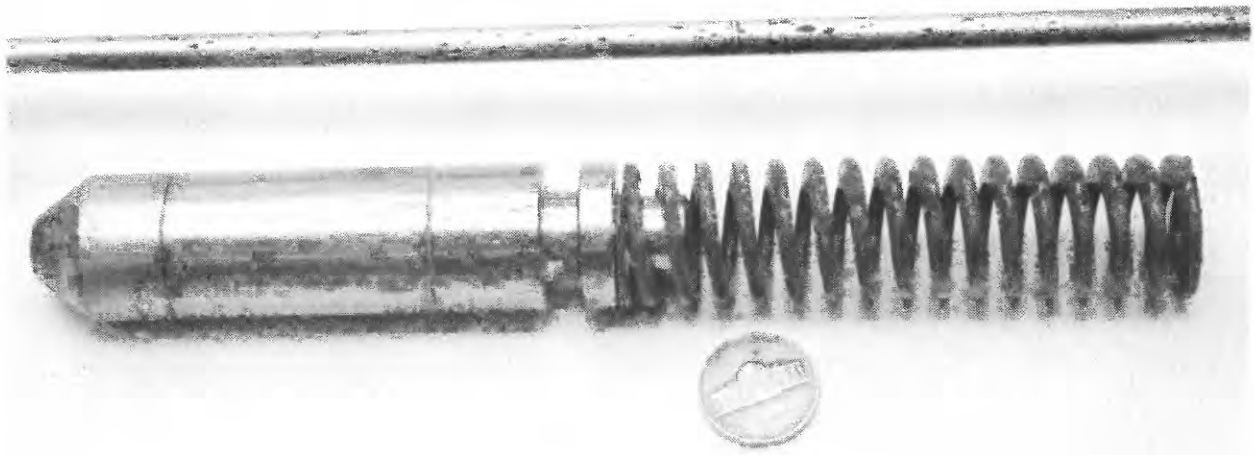

Plate II. "Grabber" assembled with return spring
(see drawing, Figure C-3),
and probe showing dimples made by grabber balls.

Plate III. Close-up of the upper section of a probe with 20 runs. Teardrop-shaped dimples are made by the "grabber" balls when the driving pressure on the piston of cross-sectional area ~ 1 in^2 (~ 600 mm^2) exceeds 2000 psi (15000 kPa).

APPENDIX D

Downhole Probe Electronics

The digital monitoring and data-gathering electronic components located in the logging vehicle are primarily those used in conventional temperature logs and field determinations of thermal conductivity using the needle probe (Moses and others, 1979). This system, illustrated schematically in Figure D-1 initiates and controls all operations involved in the heat-flow determinations.

Thermistor-resistance measurements are made using a 5 1/2 digit digital multimeter utilizing a constant current source through the unknown resistance along with a highly accurate zero and drift-correction method. Although a true four-wire resistance mode of operation would normally be used to compensate for cable resistance and/or changes in cable resistance with time, a different concept is adopted here because we have three thermistors and a heater circuit all serviced by four conductors (Figure D-2).

Two wires within the four-wire shielded cable extending from the logging vehicle to the heat-flow probe are used for thermistor-resistance measurements (Figure D-2). The three thermistors share a common wire and are sequentially switched across the pair by glass encapsulated reed relays (Plate IV) which exhibit less than 10 milliohms contact resistance. Four shielded reed relays are used in the downhole probe; three are used sequentially to read the individual thermistors; the fourth reed relay

places a short circuit across the pair, so cable resistance can be read and recorded, hence line resistance can be updated and compensated for on each sweep of measurements. Shorting of the resistance-measuring pair also provides thermistor-location synchronization owing to the over two orders of magnitude reduction of resistance from a thermistor measurement, a factor easily detected by software in the logging vehicle calculator (Figure D-1).

The electronics within the heat-flow probe consist of a self-contained battery-operated unit which is switched on prior to being lowered downhole (Figure D-2 and Plate IV). The unit incorporates a binary counter followed by a binary-to-decimal decoder. The binary counter is set up with hard wire reset after a count of three (0000 being an initial condition). The counter and decoder are of the C-MOS family for low power consumption and high noise immunity ($\geq$.45 VDD). The decimal decoder sequentially energizes four relay drivers.

The requirement to select a starting point for measurements and to control the elapsed time between thermistor readings and monitoring time is accomplished by a programmable timer (Figure D3) in the logging vehicle. In this operation (Figures D-1, D-2, and D-3) a pre-programmed interval pulse is sent down the cable (<1 ms duration) on one resistance-measurement leg and referenced to the shield. A signal conditioned, high Z Schmitt trigger within the probe housing provides the counting clock for the binary counter.

The programmable timer in the logging vehicle can be set to allow any number of thermistor-drift readings (due to penetration friction) to be made until an equilibrium is met or can be calculated by extrapolation (Figures 5 and 6). At this time, the timer energizes the heater circuit within the downhole probe by means of a contact closer in the timer. The heater-power source is derived from a high-level constant current source with excellent stability (±0.01%). This current source is set approximately to the desired value and is measured and monitored digitally by the voltage drop across a stable, precision wire-wound resistor wired in series with the source. The heater circuit is isolated completely from adjacent conductors and the shield.

Real-time data computation and processing are accomplished with various components within the logging vehicle (Figure D-1). Look-up tables are stored and accessed with a programmable calculator and applied to the data acquired by the digital multimeter. Data are stored on digital tape and on printed paper tape, and results are plotted on an X-Y plotter. Control signals, data formatting, and device handshaking are accomplished by interface components programmed to marry the individual instruments, details of which are not provided here because the rapid evolution of microprocessor technology will probably render many (if not most) of the components used in this study obsolete by the time these results are published. Off-the-shelf components can be duplicated (or improved upon) by reference to Figure D-1. The custom-designed components are shown in greater detail in Figures D-2 and D-3 and in Plate IV.

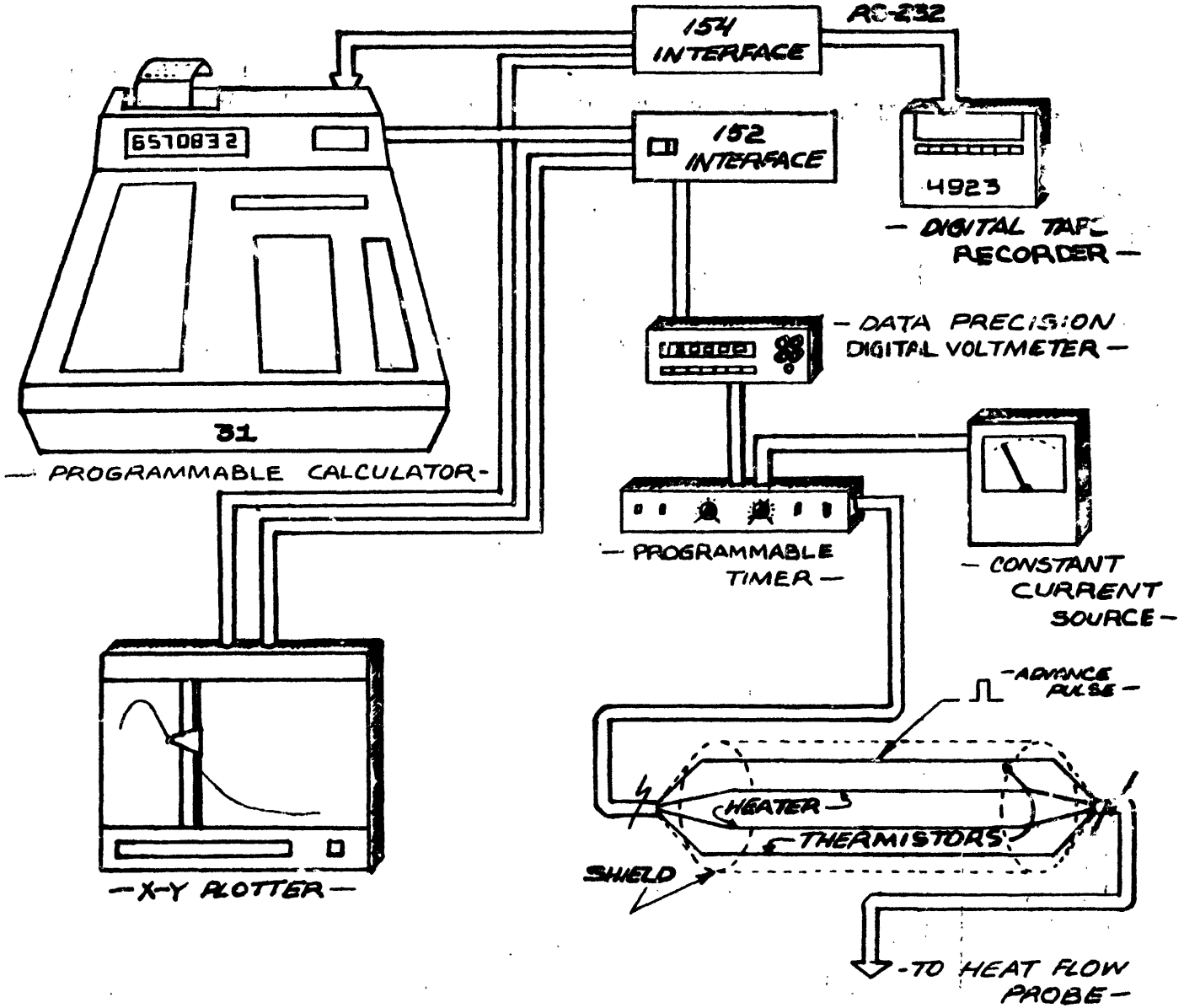

Figure D-1. Schematic diagram showing the various components of the downhole probe system.

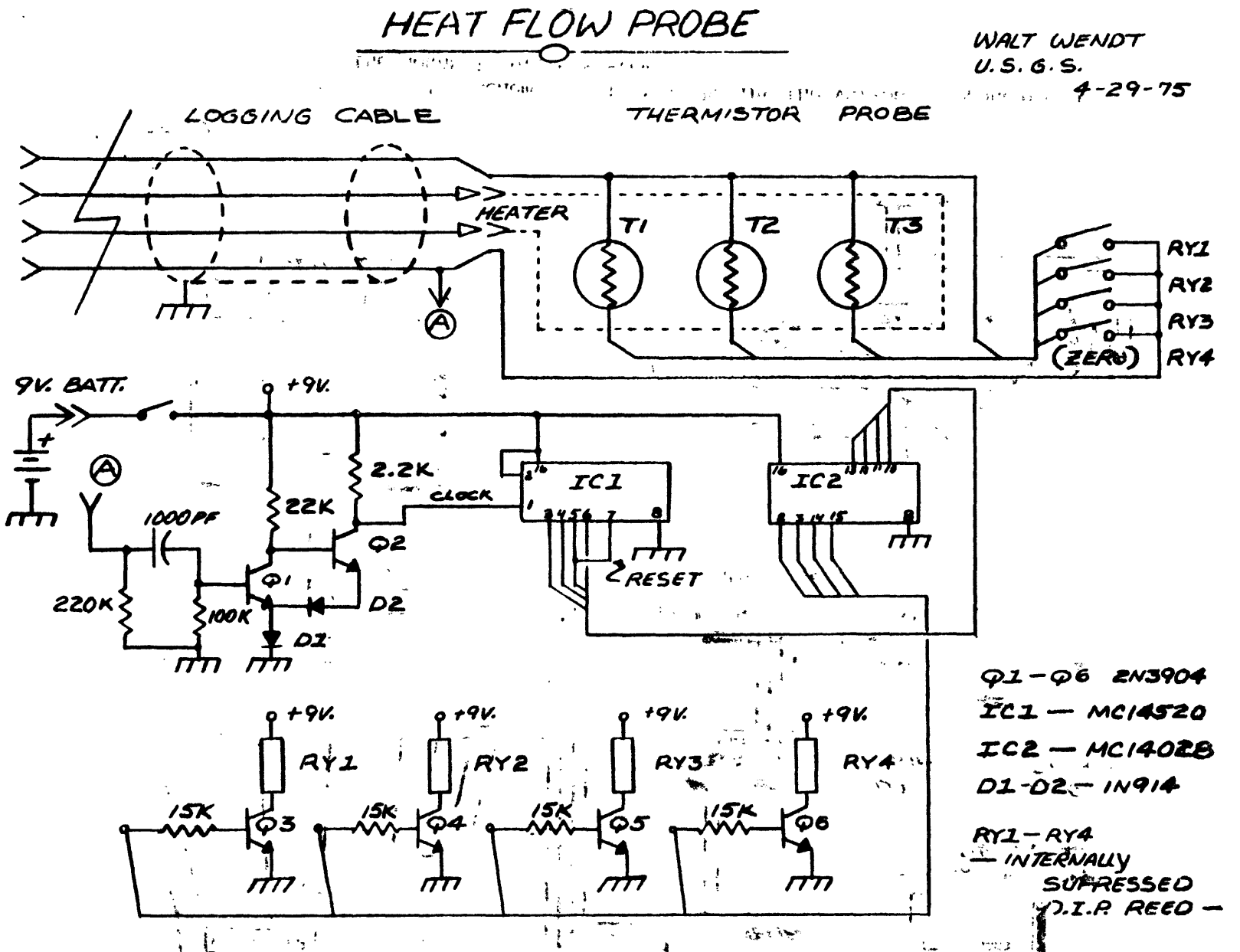

Figure D-2. Circuit diagram for the downhole switching arrangement. T1, T2, and T3 are the thermistors (1 lowermost).

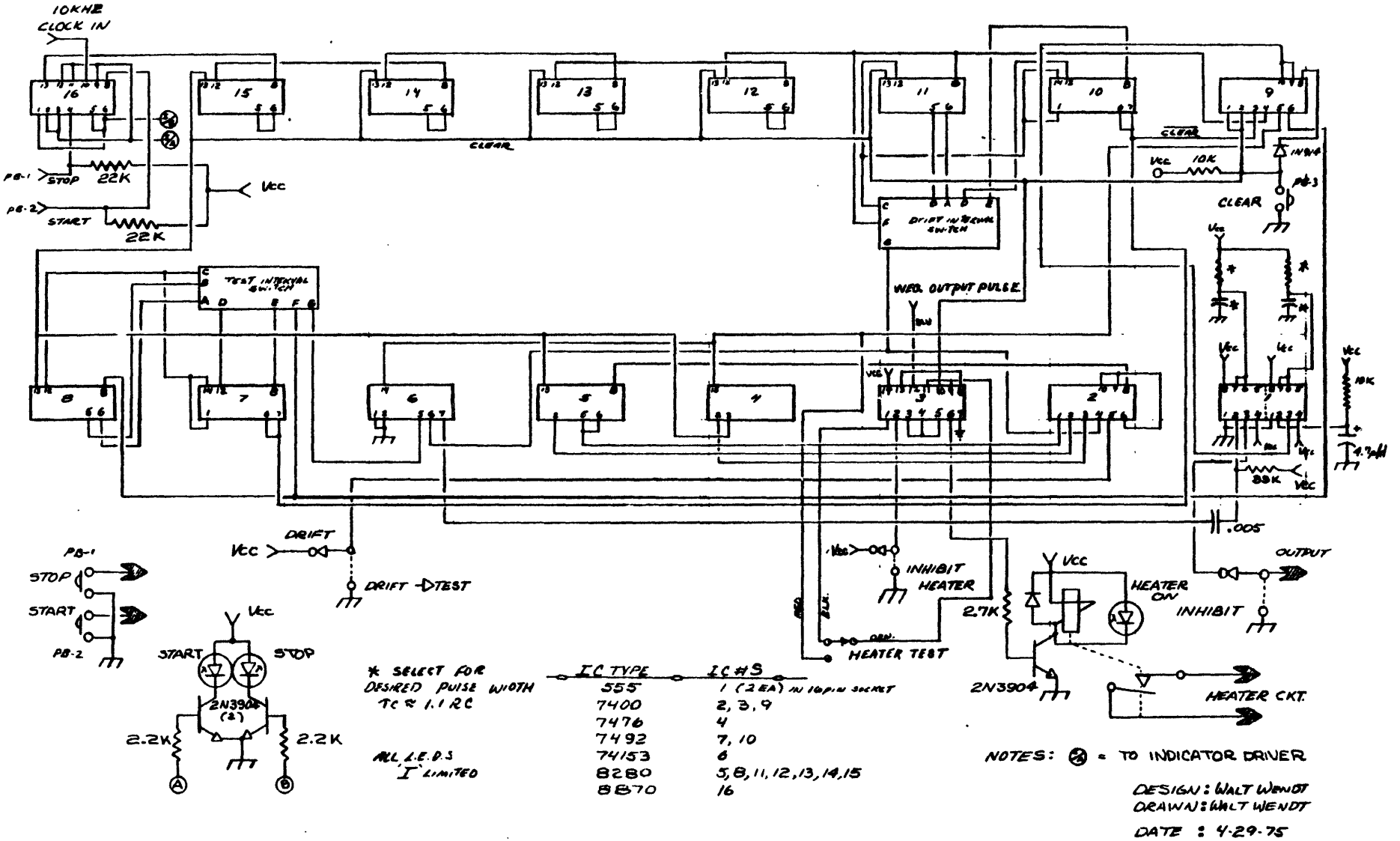

Figure D-3. Circuit diagram for programmable timer used to control both needle-probe conductivity determinations on core and downhole temperature and thermal conductivity determinations.

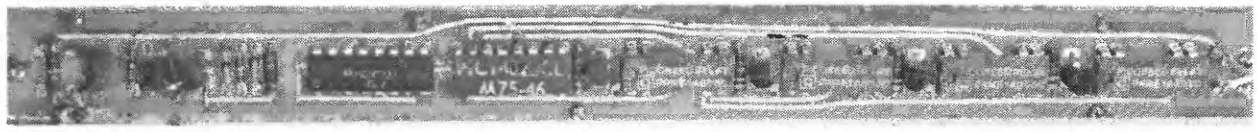

Plate IV. Physical layout of downhole switching circuitry
(see circuit diagram, Figure D-2)